VAL genes regulate vegetative phase change via miR156-dependent and independent mechanisms

Jim P. Fouracre[1], Jia He[1,3], Victoria J. Chen[1], Simone Sidoli[2] and R. Scott Poethig[1]*

[1] Biology Department, University of Pennsylvania, Philadelphia, Pennsylvania, 19104, USA

[2] Department of Biochemistry, Albert Einstein College of Medicine, Bronx, New York 10461, USA

[3] Current address: Cold Spring Harbor Laboratory, Cold Spring Harbor, New York 11724, USA

* Corresponding author: Poethig, R. S. (spoethig@sas.upenn.edu)

Abstract

How organisms control when to transition between different stages of development is a key question in biology. In plants, epigenetic silencing by Polycomb repressive complex 1 (PRC1) and PRC2 plays a crucial role in promoting developmental transitions, including from juvenile-to-adult phases of vegetative growth. PRC1/2 are known to repress the master regulator of vegetative phase change, miR156, leading to the transition to adult growth, but how this process is regulated temporally is unknown. Here we investigate whether transcription factors in the *VIVIPAROUS/ABI3-LIKE* (*VAL*) gene family provide the temporal signal for the epigenetic repression of miR156. Exploiting a novel *val1* allele, we found that *VAL1* and *VAL2* redundantly regulate vegetative phase change by controlling the overall level, rather than temporal dynamics, of miR156 expression. Furthermore, we discovered that *VAL1* and *VAL2* also act independently of miR156 to control this important developmental transition.

41 **Introduction**

42 Flowering plant development is underpinned by transitions between stereotypical
43 stages of growth: embryogenesis, seed maturation, juvenile and adult phases of
44 vegetative development and flowering (Huijser and Schmid, 2011). The correct timing of
45 these transitions is critical to plant survival and, ultimately, reproductive success.
46 Vegetative phase change describes the transition from juvenile-to-adult vegetative
47 growth and is associated with changes to multiple traits, including leaf morphology,
48 light-use efficiency, herbivore resistance and shoot physiology (Gou et al., 2011;
49 Lawrence et al., 2020; Leichty and Poethig, 2019; Mao et al., 2017). In *Arabidopsis*
50 *thaliana*, the juvenile phase is characterized by small round leaves that lack both
51 trichomes on the abaxial surface and serrations. Adult leaves, on the other hand, are
52 larger, more elongated, serrated and produce abaxial trichomes (Telfer et al., 1997).

53 Vegetative phase change is triggered by activity of members of the *SQUAMOSA*
54 *PROMOTER BINDING PROTEIN-LIKE* (*SPL*) family of transcription factors, which are
55 post-transcriptionally repressed during juvenile development by the microRNAs
56 miR156/miR157 (Fouracre and Poethig, 2019; Wu and Poethig, 2006; Wu et al., 2009;
57 Xu et al., 2016a). miR156/miR157 are encoded by multiple genes of which *MIR156A*
58 and *MIR156C* are the most functionally significant (He et al., 2018). The expression of
59 *MIR156A* and *MIR156C* declines during juvenile growth (Yang et al., 2013b; Yu et al.,
60 2013), leading to the de-repression of their *SPL* targets and the transition to adult
61 growth. Elucidating what controls the decline in *MIR156A*/*C* expression is therefore
62 critical to understanding how the juvenile-to-adult transition is regulated in plants.

63 The molecular mechanisms that lead to the temporal repression of *MIR156A/C*
64 are only beginning to be understood. The activity of Polycomb Group (PcG)
65 transcriptional repressors appears critical. There are two functional complexes of PcG
66 proteins in plants, both of which repress gene expression through covalent histone
67 modifications. PcG repressive complex 1 (PRC1) consists of a H2A E3 ubiquitin ligase
68 module containing one AtBMI1 protein (AtBMI1A/B/C) and one AtRING1 protein
69 (RING1A/B). PRC1 represses gene expression through ubiquitination of H2A
70 (H2AK119ub) (Bratzel et al., 2010; Calonje, 2014; Yang et al., 2013a). The PRC2
71 complex includes histone methyltransferases such as *CURLY LEAF* (*CLF*) and
72 *SWINGER* (*SWN*) and promotes H3 trimethylation (H3K27me3) (Chanvivattana et al.,
73 2004; Goodrich et al., 1997).
74 We have previously found that H3K27me3 increases at *MIR156A/C* in a PRC2-
75 dependent manner during juvenile development, and that vegetative phase change is
76 delayed in *swn* mutants (Xu et al., 2016b). The temporal deposition of H3K27me3 is
77 accompanied by depletion of the antagonistic H3K27ac mark that is associated with
78 active transcription. miR156 accumulation is also repressed by PRC1, as *atbmi1a/b*
79 mutants exhibit delayed vegetative phase change (Pico et al., 2015). In addition, we
80 have found that accumulation of the active histone mark H3K4me3 decreases at
81 *MIR156A/C* during vegetative development (Xu et al., 2018).
82 The findings that H3K27me3 replaces H3K27ac and H3K4me3 at *MIR156A/C*
83 over time, and that PRC1/PRC2-activity promotes vegetative phase change, led us to
84 propose that the temporal dynamics of miR156 accumulation are coordinated by
85 antagonistic patterns of active (H3K27ac, H3K4me3) and repressive (H3K27me3)

86 histone modifications (Xu et al., 2018, 2016b). In this model the stochastic removal of
87 H3K27ac/H3K4me3 facilitates the deposition of H3K27me3 and the gradual epigenetic
88 silencing of miR156. Similar mechanisms have been reported to function at other
89 developmental transitions (Yang et al., 2014). For example, during flowering, H3K27
90 deacetylation is a pre-requisite for PRC2-mediated H3K27me3 deposition at
91 *FLOWERING LOCUS C* (*FLC*) (Zeng et al., 2020), and during seed maturation, PRC1
92 promotes the exchange of H3K4me3 for H3K27me3 at *DELAY OF GERMINATION1*
93 (*DOG1*) and *ABSCISIC ACID INSENSITIVE3* (*ABI3*) (Molitor et al., 2014).
94 Although there is good evidence that *MIR156A/C* are epigenetically silenced
95 during vegetative development, how this mechanism is regulated temporally remains
96 unknown. *VIVIPAROUS/ABI3-LIKE* (*VAL*) genes are excellent candidates for temporal
97 effectors in this model. *VAL* genes encode B3 domain transcription factors that are
98 closely related to the *ABI3/FUSCA3* (*FUS3*)/*LEAFY COYTLEDON2* (*LEC2*) clade of
99 embryogenesis regulators. There are three *VAL* genes in *Arabidopsis*, of which *VAL1*
100 and *VAL2* (also known as *HSI2* and *HSL2* respectively) are the most functionally
101 important (Suzuki et al., 2007). VAL proteins repress their targets by binding to 6 base
102 pair RY-sequence motifs (CATGCA) via their B3 domain (Chen et al., 2018, 2020; Guo
103 et al., 2013; Jing et al., 2019; Qüesta et al., 2016; Suzuki et al., 1997; Yuan et al.,
104 2016).
105 A number of observations suggest that *VAL* genes might provide the temporal
106 information that coordinates vegetative phase change: 1) *VAL* genes regulate other
107 developmental transitions, i.e. seed maturation (Suzuki et al., 2007; Yang et al., 2013a)
108 and flowering (Qüesta et al., 2016; Yuan et al., 2016); 2) *MIR156A/C* expression is

109 elevated in *val1/2* mutants (Pico et al., 2015); 3) VAL1/2 physically interact with several
110 histone deacetylases (*HDA6/9/19*) (Chhun et al., 2016; Qüesta et al., 2016; Zeng et al.,
111 2020; Zhou et al., 2013); and 4) *VAL* genes promote PRC1 and PRC2-binding (Chen et
112 al., 2018; Pico et al., 2015; Qüesta et al., 2016; Yuan et al., 2020, 2016)

113 In this study we investigated whether *VAL* genes function as temporal regulators
114 of vegetative phase change. We report that reduced *VAL* activity significantly delays the
115 timing of vegetative phase change through both miR156-dependent and independent
116 mechanisms. We find that the temporal decline in miR156 expression is remarkably
117 robust and is insensitive to loss of *VAL* function, inhibition of VAL1-binding and the
118 combined loss of *VAL1* and PRC2 components. Finally, we show that the effects of
119 *VAL1* on the timing of vegetative phase cannot be explained by temporal changes in its
120 interactions with other proteins.

121

122 **Results**

123 ***VAL* genes promote vegetative phase change**

124 To investigate the role of *VAL* genes in vegetative phase change, we exploited a novel
125 mutant we identified in an ethyl methanesulfonate screen for plants exhibiting prolonged
126 juvenile development. Mapping-by-sequencing revealed a substitution at the *VAL1*
127 locus, resulting in the conversion of a highly conserved arginine residue to a cysteine in
128 the N-arm of the VAL1 B3 DNA-binding domain (Supplementary file 1A). This arginine
129 residue is critical for VAL1 binding to target RY-motifs (Sasnauskas et al., 2018). The
130 mutation in *VAL1* was confirmed to be the cause of the late juvenile phenotype by its
131 failure to complement the null *val1-2* T-DNA insertion allele, and by the ability of the

132 *VAL1* genomic sequence to rescue this phenotype (Supplementary file 1B,C). Unlike
133 *val1-2*, the novel *val1* allele is semi-dominant, and delays vegetative phase change
134 when heterozygous (Supplementary file 1D). We therefore named this new allele *val1-*
135 *5(sd)*, consistent with the nomenclature of existing *val1* alleles (Veerappan et al., 2012).
136 Both *val1-5(sd)* and *val1-2* exhibit delayed vegetative phase change, with *val1-*
137 *5(sd)* having a stronger effect on the timing of abaxial trichome production than *val1-2*
138 (Supplementary file 1B). As *VAL1* functions redundantly with *VAL2* to regulate other
139 developmental transitions (Qüesta et al., 2016; Suzuki et al., 2007; Tsukagoshi et al.,
140 2007; Yuan et al., 2016), we tested the effects of *val1; val2* double mutants on
141 vegetative phase change. Previous analyses of *VAL* gene function have utilized *val1-2;*
142 *val2-1* and *val1-2; val2-3* double mutants. However, seedling development is so strongly
143 perturbed in *val1-2; val2-1* and *val1-2; val2-3* plants (Suzuki et al., 2007; Tsukagoshi et
144 al., 2007; Yang et al., 2013a; Yuan et al., 2020) that analyses of vegetative growth is
145 problematic in these backgrounds. Therefore, we generated new *val1; val2*
146 combinations using *val2-3* and a previously uncharacterized T-DNA insertion allele we
147 named *val2-4* (Figure 1A). Consistent with previous studies (Suzuki et al., 2007;
148 Tsukagoshi et al., 2007; Yuan et al., 2016), *val2* single mutants had no discernible
149 effect on vegetative phase change (Figure 1B, Supplementary file 1E). However, loss of
150 *VAL2* activity enhanced the phenotypes of *val1-2* and *val1-5(sd)*. *val1-2; val2-4* and
151 *val1-5(sd); val2-3* both exhibited delayed abaxial trichome production relative to *val1-2*
152 and *val1-5(sd)*, respectively (Figure 1C). *val1-5(sd)*; *val2-3* flowered significantly later
153 than *val1-5(sd)* (Figure 1D) and *val1-2; val2-4* produced leaves that were significantly
154 more juvenile in shape (i.e. rounder) than *val1-2* (Figure 1E). Neither double mutant

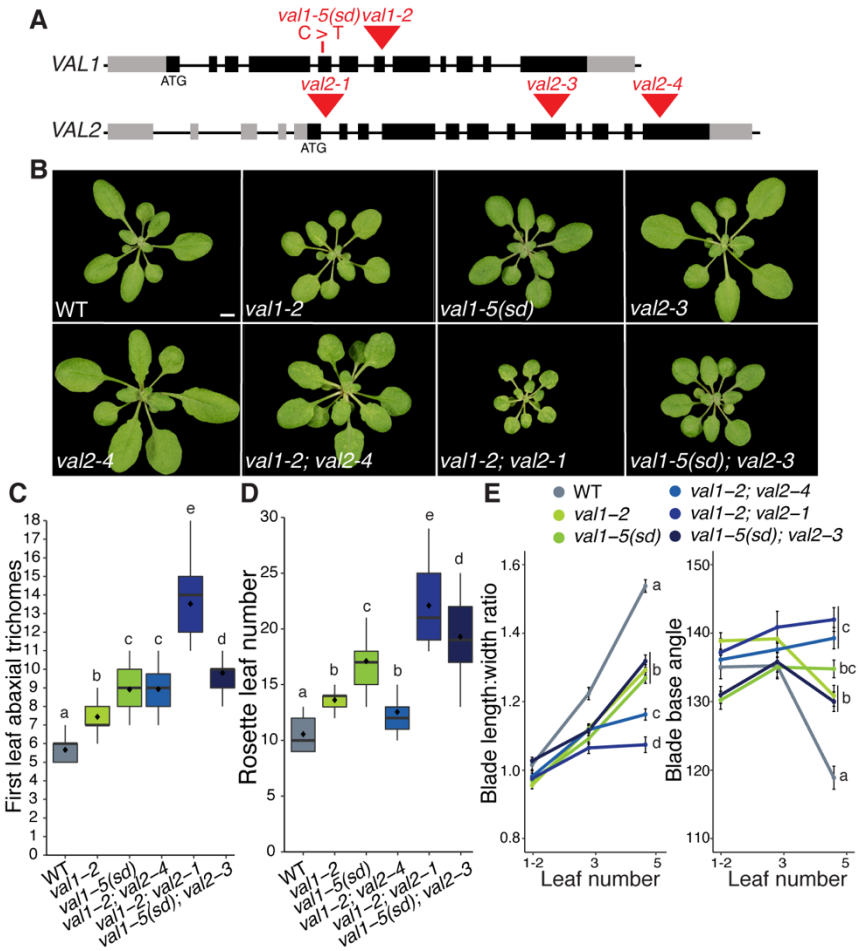

155 **Figure 1. *VAL* genes redundantly regulate vegetative phase change**

156 (A) Schematic of *val1* and *val2* alleles used in this study – grey boxes represent
157 UTRs, black boxes represent exons, red triangles represent T-DNA insertions,
158 red line represents EMS-induced base substitution.
159 (B) Phenotypes at 21 DAG in LD conditions, scale bar = 5mm.
160 (C-E) Quantitative analysis of vegetative development. Statistically distinct genotypes
161 were identified by one-way ANOVA with *post hoc* Tukey multiple comparison test
162 (letters indicate statistically distinct groups $P < 0.05$; for (E) comparisons were
163 made at leaf 5), all plants grown in LD. (C,D) Boxes display the interquartile
164 range (IQR) (boxes), median (lines) and values beyond 1.5*IQR (whiskers);
165 mean values are marked by ◆. (E) Colored lines represent the mean and black
166 bars the SEM. Sample sizes (C, D) 21-46, (E) 13-46.
167

168 combination was as phenotypically severe as *val1-2; val2-1* (Figure 1C-E). The weaker
169 phenotype of *val1-5(sd); val2-3* than *val1-2; val2-3* (Yang et al., 2013a; Yuan et al.,
170 2020) suggests that the semi-dominant phenotype of *val1-5(sd)* is mediated by
171 interaction with *VAL2*. Importantly, the rate of germination was higher in *val1-2; val2-4*
172 and *val1-5(sd); val2-3* relative to existing *val1; val2* double mutants. *val1-2; val2-4* and
173 *val1-5(sd); val2-3* thus provide a balance between phenotypic strength and
174 experimental viability and are useful tools for investigating the role of *VAL* genes in
175 developmental timing.
176

177 ***VAL* genes function predominantly as quantitative – rather than temporal –**
178 **regulators of miR156 expression**

179 Vegetative phase change results from a temporal decline in miR156 expression (Wu
180 and Poethig, 2006). A previous analysis of *val1-2; val2-1* revealed elevated expression
181 of *MIR156A/C* at a single time point (Pico et al., 2015). To determine whether the delay
182 in vegetative phase change we observed in *val* mutants is associated with a general
183 increase in the level of miR156, or with a delay in the decline in this miRNA, we
184 quantified miR156 expression in the shoot apex and in isolated leaf primordia at
185 different times in shoot development. The primary transcripts of *MIR156A* and *MIR156C*
186 were expressed at similar levels, and exhibited a similar temporal expression pattern, in
187 wild type, *val1-5(sd)* (Figure 2A,B) and *val1-2* shoot apices and leaf primordia
188 (Supplementary file 2). However, the abundance of the mature miR156 miRNA
189 transcript was significantly higher in *val1-5(sd)* leaf primordia than in wild type (Figure
190 2B), and it was also marginally higher in *val1-5(sd)* shoot apices than in wild type

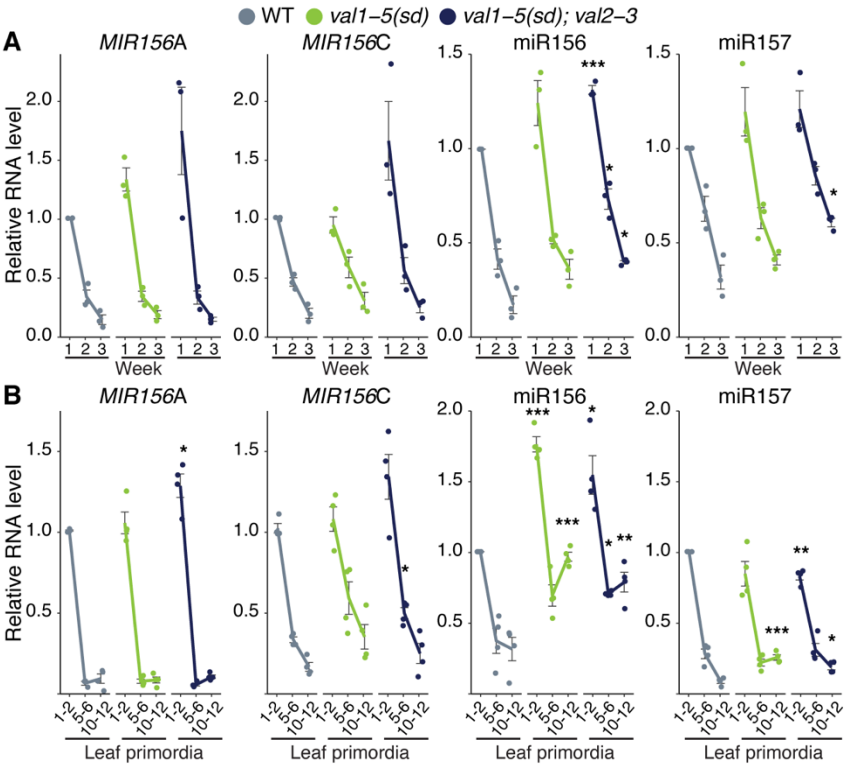

Figure 2. *VAL* genes function predominantly as quantitative regulators of miR156 expression

(A, B) qRT-PCR analyses of gene expression. (A) Shoot apices with leaf primordia (LP) ≥ 1mm removed at 1, 2 and 3 weeks. (B) Isolated LP 0.5-1mm in size. All plants were grown in SD conditions. Each data point represents a biological replicate and is the average of three technical replicates. Coloured lines represent the mean and black bars mean±s.e.m. Asterisks represent significant differences between WT and *val* mutants at the same time point, calculated by an unpaired two-tailed *t*-test with a Bonferroni correction for multiple comparisons (* $P < 0.025$; ** $P < 0.005$; *** $P < 0.0005$).

204 (Figure 2A). The *val1-5(sd); val2-3* (Figure 2A,B) and *val1-2; val2-1* (Supplementary file
205 2) double mutants had stronger effects on *MIR156A* and *MIR156C* expression than the
206 respective *val1* single mutants, suggesting that *VAL1* and *VAL2* function redundantly to
207 repress *MIR156A* and *MIR156C* transcription. Mature miR156 was elevated throughout
208 development in both the shoot apices (Figure 2A) and the leaf primordia (Figure 2B) of
209 *val1-5(sd); val2-3* double mutants. Loss of *VAL* activity also produced a slight increase
210 in miR157 levels (Figure 2A,B, Supplementary file 2). Although *val1-5(sd); val2-3*
211 increased the abundance of miR156/miR157, it had only a minor effect on the temporal
212 expression patterns of these miRNAs. For example, miR156 expression decreased
213 2.36-fold between 1W and 2W and 2.31-fold between 2W and 3W in wild type plants,
214 but decreased 1.77 and 1.82-fold between the same time points in *val1-5(sd); val2-3*
215 plants (Figure 2A). Taken together, these data suggest that *VAL* genes function
216 primarily as general, rather than temporal, regulators of miR156 expression.
217

218 **_VAL_ genes coordinate PRC1 and PRC2 recruitment at _MIR156_ loci**

219 We have previously demonstrated that the temporal decline in *MIR156A* and *MIR156C*
220 expression is associated with PRC2-dependent and progressive deposition of
221 H3K27me3 at these loci (Xu et al., 2016b). To determine if *VAL* genes contribute to this
222 process, we examined PRC2 activity in the *val1-5(sd); val2-3* double mutant. As
223 previously reported (Xu et al., 2016b), H3K27me3 levels increased at the *MIR156A* and
224 *MIR156C* loci during vegetative development in wild type plants (Figure 3A,B). Although
225 there was no difference in the temporal pattern of H3K27me3 deposition at *MIR156A* in

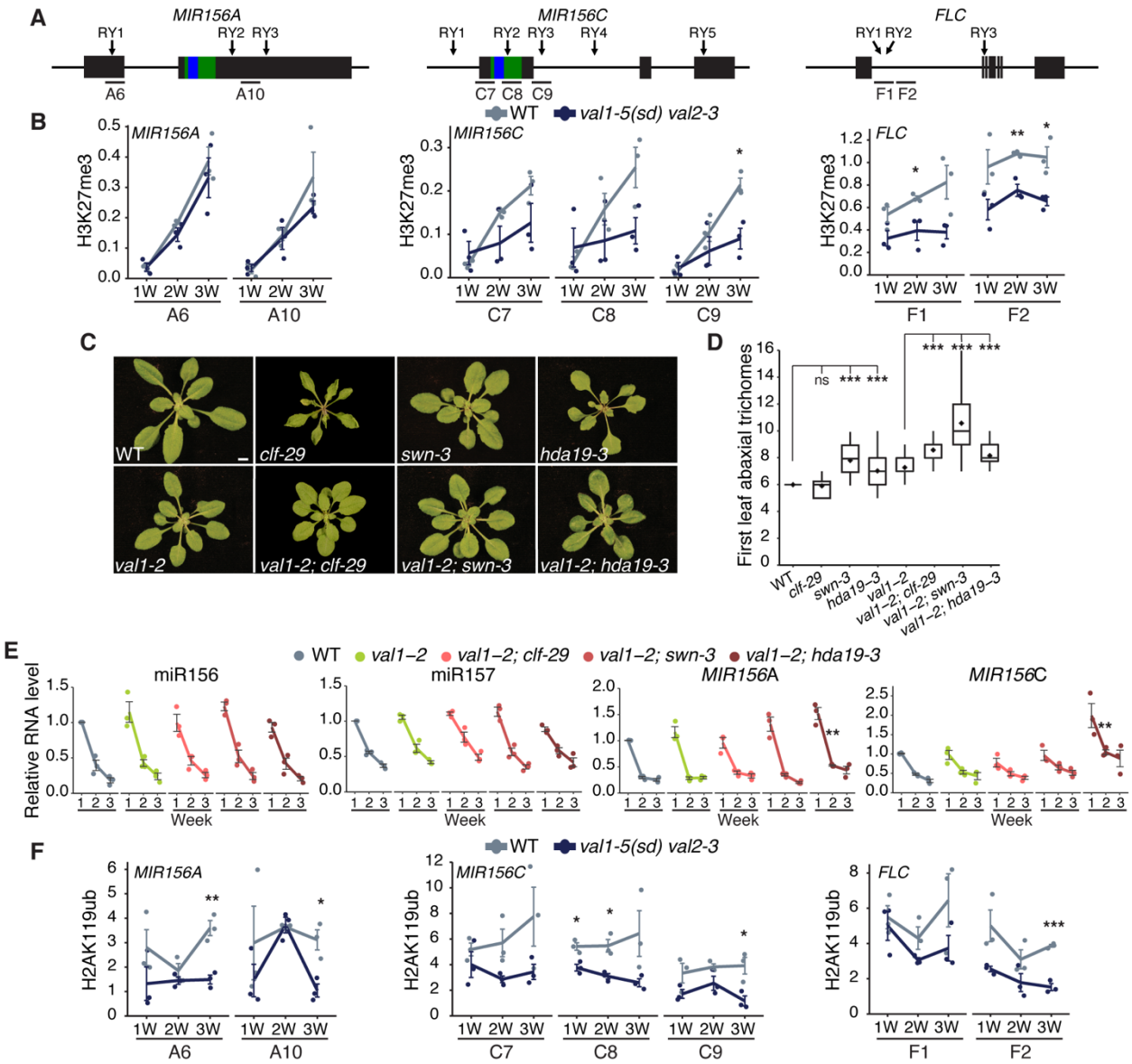

Figure 3. *VAL* genes regulate miR156 activity via-PRC2 and PRC1

(A) Schematics of the primer locations used for ChIP-qPCR. Blue and green bars represent sequences encoding the mature miRNA and miRNA hairpin respectively.

(B) Temporal analysis of H3K27me3 by ChIP-qPCR. Each data point represents a biological replicate and is the average of three technical replicates. Lines represent the mean, bars represent the mean±s.e.m., asterisks represent significant differences between WT and *val1-5(sd); val2-3* at the same time point, calculated by an unpaired two-tailed *t*-test (* $P < 0.05$; ** $P < 0.01$; *** $P < 0.001$). H3K2me3 values are relative to H3 and normalised to *STM* as an internal control. Plants were grown in SD conditions.

239 (C, D) Phenotypes in LD. (D) Photographs taken at 21DAG, scale bar = 5mm. (E)
240 Asterisks represent significant differences to either WT or *val1-2*, calculated by
241 unpaired two-tailed *t*-test with Bonferroni correction for multiple comparisons (***
242 $P < 0.00033$). Sample size 22-46.
243 (E) qRT-PCR analyses of gene expression in shoot apices with LP ≥ 1mm removed
244 at 1, 2 and 3 weeks. Each data point represents a biological replicated and is the
245 average of three technical replicates. Coloured lines represent the mean and
246 black bars represent the mean±s.e.m. Asterisks represent significant differences
247 between *val1-2* and *val1-2; clf-29/val1-2; swn-3/val1-2; hda19-3* at the same time
248 point, calculated by unpaired two-tailed *t*-test with Bonferroni correction for
249 multiple comparisons (** $P < 0.0033$). Plants were grown in SD conditions.
250 (F) Temporal analysis of H2AK119ub by ChIP-qPCR, values are relative to input and
251 normalised to *ACT7* as an internal control. See (B) for details.
252

253 *val1-5(sd); val2-3*, the rate of H3K27me3 deposition at *MIR156C* was significantly
254 slower in this double mutant (Figure 3B). These results are consistent with a recent
255 genome-wide study that revealed a decrease in H3K27me3 levels at *MIR156C*, but not
256 *MIR156A*, in *val1-2; val2-3* plants (Yuan et al., 2020). As a control, we measured
257 H3K27me3 deposition at the floral regulator *FLC.* In the absence of vernalization, we
258 observed no change in the level of H3K27me3 during vegetative development in wild
259 type plants (Figure 3B). However, consistent with previous reports (Qüesta et al., 2016;
260 Yuan et al., 2016), there was a significant decrease in H3K27me3 at *FLC* in *val1-5(sd);*
261 *val2-3*.
262 *VAL1* is thought to act by recruiting PRC1 which, in turn, promotes the activity of
263 PRC2 (Baile et al., 2020; Calonje, 2014; Zhou et al., 2017). As a genetic test of this
264 hypothesis, we examined the interaction between *val1-2* and *clf-29* and *swn-3,* loss-of-
265 function mutations in the functionally redundant genes that encode the histone
266 methyltransferase activity of PRC2. As we have shown previously (Xu et al., 2016b),
267 *swn-3* had a larger effect on the timing of vegetative phase change than *clf-29* (Figure
268 3C,D). Consistent with the hypothesis that *VAL1* regulates vegetative phase via its
269 effect on PRC2 activity, *clf-29* and *swn-3* interacted synergistically with *val1-2,* in that
270 the double mutants had a much more severe vegetative phase change phenotype than
271 the single mutants (Figure 3C,D). Notably, *val1-2* suppressed the curling leaf phenotype
272 of *clf-29* (Figure 3C), presumably because it enhances *FLC* expression (Lopez-Vernaza
273 et al., 2012). We also examined the interaction between *val1-2* and *hda19-3*, a putative
274 null allele of the histone deacetylase HDA19. *hda19-3* is predicted to delay vegetative
275 phase change because *HDA19* is required for PRC2-mediated repression (Zeng et al.,

276 2020), HDA19 physically interacts with VAL1 (Qüesta et al., 2016) and loss-of *HDA19*
277 enhances H3K4me3 levels (Jang et al., 2011). As predicted, *hda19-3* produced abaxial
278 trichomes significantly later than wild type (Figure 3D), and *val1-2; hda19-3* double
279 mutants produced abaxial trichomes significantly later than either single mutant.
280 Together, these results suggest that *val* mutations delay vegetative phase change by
281 interfering with the activity of PRC2.

282 To determine whether the synergistic interaction between *clf-29, swn-3, hda19-3*
283 and *val1-2* is due to enhanced miR156/miR157 expression, we quantified expression of
284 the mature miR156 and miR157 miRNAs, and the primary *MIR156A* and *MIR156C*
285 transcripts, in these mutant backgrounds. The overall level and expression pattern of
286 the mature miR156/miR157 transcripts were not affected by *val1-2*, or by *val1-2; clf-29*,
287 *val1-2; swn-3*, and *val1-2; hda19-3* double mutants (Figure 3E). However, *pri-MIR156A*
288 and *pri-MIR156C* transcripts were significantly elevated in *val1-2; hda19-3,* although the
289 rate of decline in the expression of these transcripts was normal. The lack of correlation
290 between the expression of miR156 and the level of *pri-MIR156A* and *pri-MIR156C* is
291 surprising given that these loci are the major sources of miR156. One possibility is that
292 the miRNA processing pathway is compensating for elevated levels of the primary
293 transcripts. In any case, these results suggest that *VAL* genes temporally regulate the
294 deposition of H3K27me3 at specific *MIR156* loci, but are not necessary for the temporal
295 decline in miR156 expression.

296 *VAL* genes also repress gene expression by promoting H2AK119ub deposition
297 via recruitment of PRC1 (Yang et al., 2013a). Unlike H3K27me3 (Figure 3B) (Xu et al.,
298 2016b), we found no evidence that H2AK119ub increases over time at *MIR156A* and

299 *MIR156C* (Figure 3F). However, we did find that *val1-5(sd); val2-3* had significantly
300 lower levels of H2AK119ub than wild type plants. This effect was observed throughout
301 development at *MIR156C*, but seemed to be limited to later in development at
302 *MIR156A*. Importantly, *val1-5(sd); val2-3* had significantly reduced levels of H2AK119ub
303 at *MIR156C* one week after planting, which is before a difference in H3K27me3 is
304 detectable at this locus (Figure 3B). *val1-5(sd); val2-3* also had reduced levels of
305 H2AK119ub at *FLC* (Figure 3F).
306

307 ***VAL1* regulates vegetative phase change via miR156-dependent and miR156-**
308 **independent mechanisms**

309 To investigate whether the effects of *val1-5(sd); val2-3* on the chromatin state of
310 *MIR156A/C* are due to a direct regulatory interaction, we carried out chromatin-
311 immunoprecipitation qPCR using an HA-tagged version of VAL1 (Qüesta et al., 2016).
312 Confirming the results of a recent ChIP-seq study (Yuan et al., 2020), we found VAL1-
313 binding at specific locations within both the *MIR156A* and *MIR156C* loci (Figure 4A,B,
314 Supplementary file 3). The affinity of VAL1 for *MIR156A/C* appeared consistent
315 throughout vegetative development. VAL1/2 bind to RY-sequence motifs, of which there
316 are multiple copies in both *MIR156A* and *MIR156C* (Figure 4A). To determine if these
317 RY-sites are required for the regulation of vegetative phase change, we mutated 5 RY-
318 sites in *MIR156C* individually and in combination. We selected *MIR156C* because it is
319 more sensitive to *VAL* activity than *MIR156A* (Figure 2,3, Supplementary file 2). A C>T
320 substitution that eliminates VAL1 binding (Sasnauskas et al., 2018) was introduced in
321 one or all of these sites in a genomic construct of *MIR156C*. Wild type and mutant

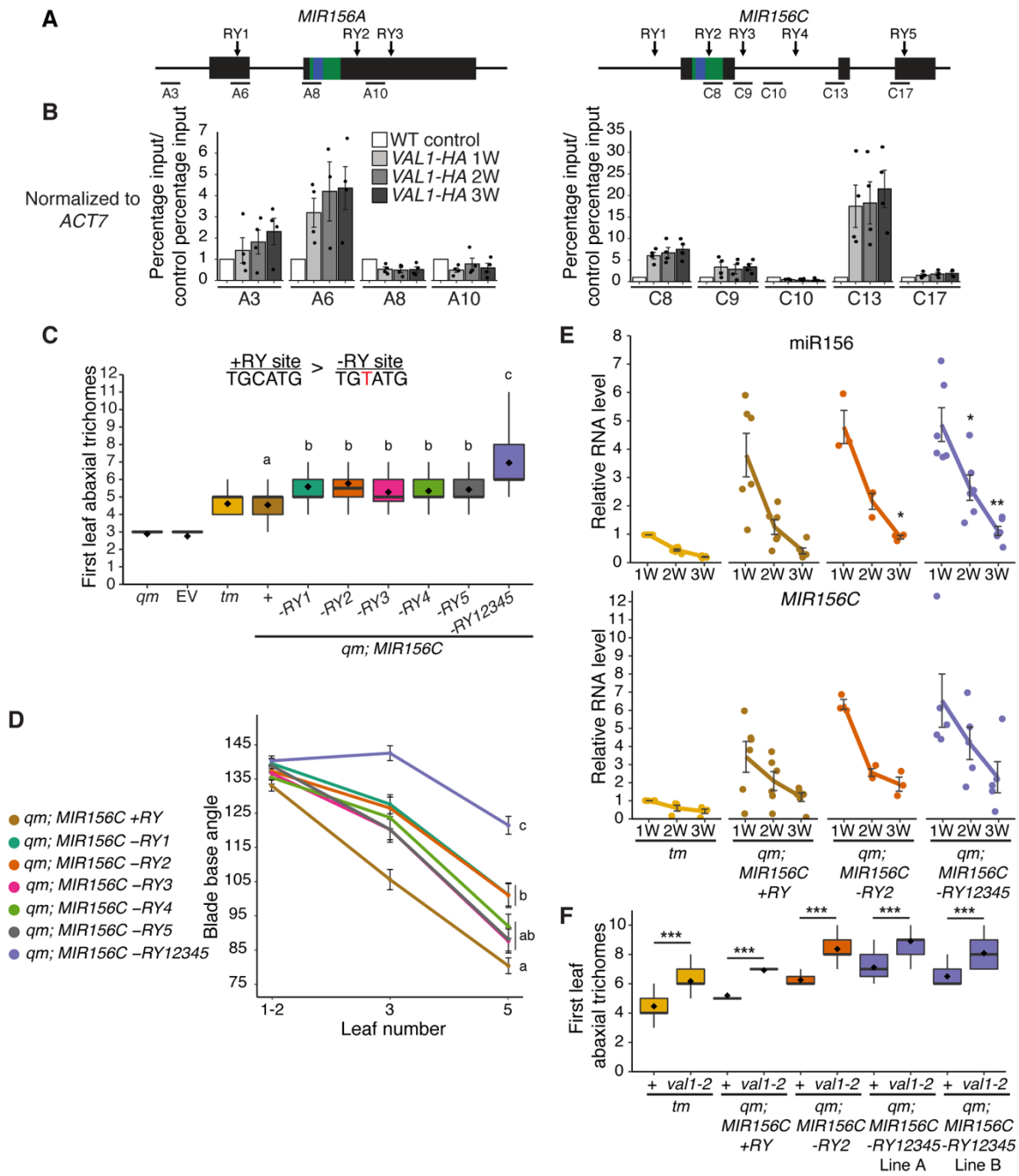

Figure 4. Loss of RY VAL-binding motifs at the *MIR156C* locus delays vegetative phase change

(A) Schematic depicting the location of primers used for ChIP-qPCR, the sequences encoding the miR156 hairpin and mature miRNA are coloured green and blue respectively.

(B) Anti-HA ChIP-qPCR of WT Col control plants at 2W and *VAL1::VAL1-HA; val1-2; FRI-Sf2* plants at 1, 2 and 3W of growth. The data is presented as percentage input normalized to *ACT7* and is displayed relative to WT. Each data point represents a biological replicate and is the average of three technical replicates, bars represent the mean and error bars the mean±s.e.m.

333 (C, D) Phenotypes of T1 plants transformed with *MIR156C* RY variants. Statistically
334 distinct genotypes were identified by one-way ANOVA with *post hoc* Tukey
335 multiple comparison test (letters indicate statistically distinct groups $P < 0.05$;
336 comparison in (C) made at leaf 5). *qm = mir156a mir156c mir157a mir157c*
337 *quadruple mutant, tm = mir156a mir157a mir157c triple mutant,* EV = empty
338 vector. (C) Colored lines represent the mean and black bars the mean±s.e.m.
339 Sample size (B) 26-52, (C) 37-51.
340 (E) qRT-PCR analyses of gene expression in shoot apices with LP ≥ 1mm removed
341 at 1, 2 and 3 weeks. Each data point represents an independent homozygous T3
342 line and is the average of three technical replicates. Colored lines represent the
343 mean and black bars the mean±s.e.m. Asterisks represent significant differences
344 between *qm; MIR156C* and *qm; MIR156C -RY* lines at the same time point,
345 calculated by an unpaired two-tailed *t*-test with a Bonferroni correction for
346 multiple comparisons (* $P < 0.025$, ** $P < 0.005$).
347 (F) Genetic interaction between *val1-2* and *MIR156C* RY deletions. Asterisks
348 represent significant differences between plants with wild type or null *VAL1*
349 alleles calculated by an unpaired two-tailed *t*-test (*** $P < 0.001$). Sample size
350 24-36. Phenotyping analyses were carried out in LD conditions, gene expression
351 and ChIP analyses were carried out in SD conditions.
352

353 constructs were then transformed into a *mir156a; mir156c; mir157a; mir157c quadruple*
354 *mutant* (*qm*) background. We chose this background because endogenous
355 miR156/miR157 activity has been largely eliminated and it is therefore sensitive to small
356 changes in the level of miR156 (He et al., 2018). Plants transformed with a wild type
357 *MIR156C* construct (+*RY*) produced leaves with abaxial trichomes at the same node as
358 the *mir156a; mir157a; mir157c triple mutant tm* (Figure 4C). *tm* has an endogenous
359 copy of *MIR156C*, confirming that the transgenic *MIR156C* sequence is fully functional.
360 Deletion of individual RY-sites produced a significant delay in the timing of abaxial
361 trichome production relative to *MIR156C +RY*, and deletion of all 5 RY-sites produced a
362 more significant delay than deletion of any single site (Figure 4C). A similar result was
363 obtained in the case of the angle of the leaf base (Figure 4D). These results
364 demonstrate that all five RY-sites are important for the expression of *MIR156C*, and that
365 they function additively. Individual RY-sites have also been shown to interact additively
366 to repress the VAL1-PRC2 targets *FLC* and *DOG1* (Chen et al., 2020; Yuan et al.,
367 2016).

368 To determine if these phenotypic effects are due to altered *MIR156C* expression,
369 we quantified miR156 levels in *MIR156C +RY, MIR156C -RY2* and *MIR156C -RY12345*
370 plants. *MIR156C -RY2* was selected because it has a marginally stronger effect than
371 other individual -RY deletions (Figure 4C,D). Although there was considerable variation
372 in miR156 levels between independent transgenic lines, *MIR156C -RY2* and *MIR156C -*
373 *RY12345* plants had significantly more miR156 than plants transformed with *MIR156C*
374 *+RY* (Figure 4E, Supplementary file 4). However, the temporal expression pattern of
375 *MIR156C* was identical in -*RY* and +*RY* plants.

376 To establish whether the effects of RY-deletion are *VAL1*-dependent, we crossed
377 *val1-2* into the *qm; MIR156C +/-RY* lines. If the delay in vegetative phase change in
378 *MIR156C -RY* lines is a consequence of reduced VAL1 binding, *val1-2* should have less
379 effect in *MIR156C -RY* lines than in *MIR156C +RY* lines or the *tm*, in which RY sites are
380 intact. Surprisingly, we found that loss-of *VAL1* significantly delayed abaxial trichome
381 production in *MIR156C -RY* as well as *MIR156C +RY* and *tm* plants (Figure 4F). It is
382 possible that *MIR156C* RY-sites are bound by other B3 domain transcription factors.
383 However, RY-binding is restricted to the *ABI3/FUS3/LEC2* and *VAL* clade of B3 domain
384 genes (Kagaya et al., 1999; Sasnauskas et al., 2018; Yuan et al., 2016). The
385 expression of *ABI3/FUS3/LEC2* is largely restricted to seed development (Carbonero et
386 al., 2017) and therefore these genes are unlikely to regulate vegetative shoot identity.
387 Moreover, FUS3 and ABI3 directly promote the expression of *MIR156C* (Tian et al.,
388 2020; Wang and Perry, 2013). A role for these genes in the regulation of *MIR156C* post-
389 germination is thus inconsistent with the juvenilized phenotype and elevated miR156
390 expression we found in *MIR156C -RY* plants. (Figure 4C-E). With regard to the potential
391 effects of other *VAL* genes, we observed no vegetative phase change phenotype in *val2*
392 single mutants (Figure 1B, Supplementary file 1E) and *VAL3* has limited expression and
393 functionality relative to *VAL1* and *VAL2* (Suzuki et al., 2007). Alternatively, this result
394 suggests that *VAL1* may regulate vegetative phase change through both miR156-
395 dependent and miR156-independent mechanisms. This interpretation is supported by
396 the observation that loss-of *VAL1* and PRC2-components strongly delayed vegetative
397 phase change but had only minor effects on miR156 expression (Figure 3C-E).

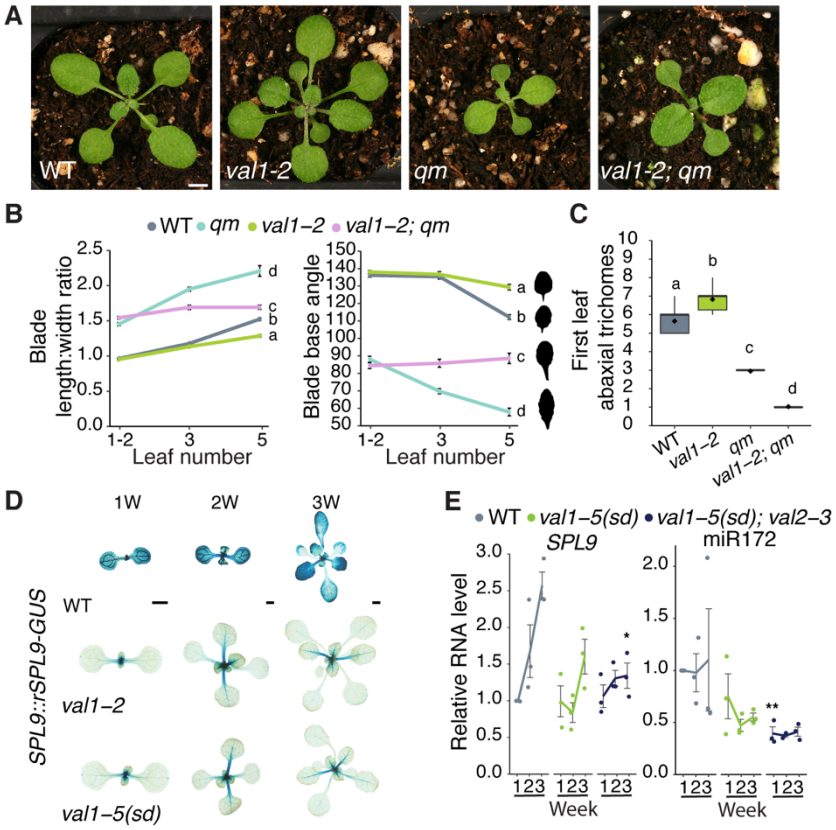

Figure 5. *VAL1* regulates vegetative phase change by miR156-dependent and independent mechanisms

(A-C) Phenotypes of *val1-2* and *mir156a mir156c mir157a mir157c quadruple mutant* lines. (A) Photographs taken at 17 DAG. Scale bar = 1mm. (B, C) Statistically distinct genotypes were identified by one-way ANOVA with *post hoc* Tukey multiple comparison test (letters indicate statistically distinct groups $P < 0.05$; (B) comparisons made at leaf 5). Bars represent the mean±s.e.m. Sample size (B) 17-60, (C) 18-36. Silhouettes in B show representative leaf 5 shapes.

(D) Expression of a miR156-resistant (*rSPL9*) reporter construct in WT, *val1-2* and *val1-5(sd)* backgrounds. Scale bars = 1mm.

(E) qRT-PCR analysis of gene expression in shoot apices with LP ≥ 1mm removed at 1, 2 and 3 weeks. Each data point represents a biological replicate and is the average of three technical replicates. Coloured lines represent the mean and gray bars represent the mean±s.e.m. Asterisk represents significant difference between WT and *val* mutant lines at the same time point, calculated by an unpaired two-tailed *t*-test with a Bonferroni correction (* $P < 0.025$; ** $P < 0.005$). All phenotypic analyses were carried out in LD conditions, the gene expression analysis was carried out in SD conditions.

418 To test this hypothesis, we introgressed *val1-2* into the *qm* genetic background,
419 which has very low levels of miR156/miR157 (He et al., 2018). Although the gross
420 morphology (Figure 5A) of *val1-2*; *qm* seedlings was indistinguishable from that of *qm*
421 plants, *val1-2* partially suppressed the effect of the *qm* genotype on the morphology of
422 leaves 3 and 5 (Figure 5B). This confirms that *VAL1* functions through a
423 miR156/miR157-independent mechanism to regulate vegetative phase change.
424 Surprisingly, a survey of abaxial trichome production revealed that *val1-2* enhanced this
425 aspect of the precocious *qm* phenotype (Figure 5C). This result can be explained given
426 that reduced histone deacetylation in a *toe* loss-of-function background accelerates
427 abaxial trichome formation (Wang et al., 2019), that *SPL* genes repress *TOE* activity
428 (Wu et al., 2009), and that *VAL* genes promote histone deacetylation (Zeng et al., 2020;
429 Zhou et al., 2013).
430 To determine if *VAL1* regulates *SPL* gene expression independently of miR156,
431 we crossed a miR156-resistant (*rSPL9*) *SPL9::rSPL9-GUS* reporter construct into *val1*
432 genetic backgrounds. The expression of this reporter was visibly and strongly
433 suppressed by *val1-2* and *val1-5(sd*) (Figure 5D), implying that miR156 is not required
434 for the regulation of *SPL9* by *VAL1*. The transcript levels of *SPL9*, and its target
435 miR172, were also decreased in *val* mutant plants (Figure 5E). However, it is difficult to
436 know if this decrease is dependent or independent of miR156 because miR156 induces
437 cleavage of the *SPL9* transcript (German et al., 2008; He et al., 2018; Ronemus et al.,
438 2006).
439 VAL1/2 act as transcriptional repressors. As *SPL9* transcription decreases in *val*
440 loss-of function mutants it is therefore unlikely that VAL1/2 regulate *SPL9* directly. To

441 test this prediction, we quantified H2AK119ub and H3K27me3 at *SPL9.* Consistent with
442 previous studies, we found high levels of H2AK119ub but negligible H3K27me3 at *SPL9*
443 (Supplementary file 5) (Li et al., 2017; Zhou et al., 2017). We also found no difference in
444 the abundance of these modifications in wild type and *val1-5(sd); val2-3* plants. Taken
445 together these results suggest that, in addition to repressing *SPL9* via their effect on
446 miR156 levels, VAL1/2 repress *SPL9* indirectly through one or more miR156-
447 independent mechanisms. The observation that *val1-5(sd); val2-3* has no effect on
448 H2AK119ub at *SPL9* also suggests that *VAL1/2* are not universally required for PRC1-
449 activity.
450

451 **The effects of *VAL1* on developmental timing may be partly explained by its**
452 **expression pattern**

453 Our results show that *VAL* genes control the timing of vegetative phase change (Figure
454 1C,E), and have subtle effects on the expression pattern of miR156 during vegetative
455 development (Figure 2, Supplementary file 2). To determine if these effects are
456 attributable to changes in the expression level of *VAL1*, we measured the abundance of
457 *VAL1* transcript levels during vegetative growth. We observed a small but significant
458 increase in *VAL1* transcripts in shoot apices between 2 and 3 weeks of growth (Figure
459 6A) but there was no significant change in *VAL1* levels in leaf primordia (Figure 6B). To
460 further investigate *VAL1* expression over time, we generated a *VAL1* transcriptional
461 reporter by fusing a 2.3kb sequence containing the *VAL1* promoter and 5' UTR, and a
462 2kb sequence containing the *VAL1* 3'UTR and terminator, to the GUS coding sequence
463 (*VAL1::GUS-VAL1 3' UTR)*. We generated a *VAL1* translational fusion by inserting a

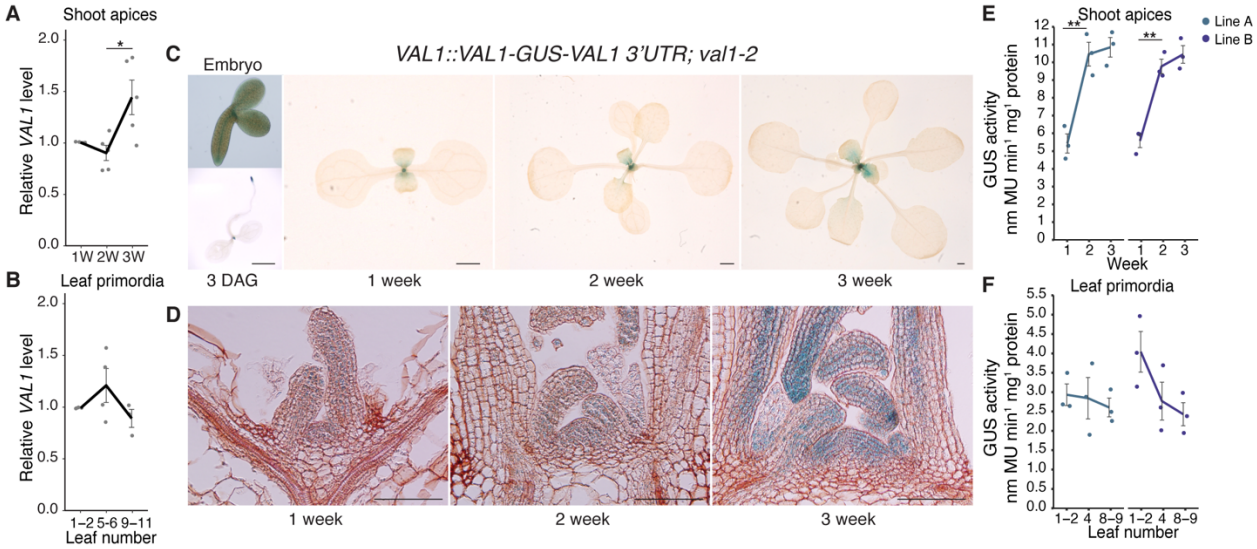

Figure 6. *VAL1* is expressed throughout vegetative development

(A, B) qRT-PCR analyses of gene expression. (A) Shoot apices with leaf primordia (LP) ≥ 1mm removed at 1, 2 and 3 weeks. (B) Isolated LP 0.5-1mm in size.

(C-F) Analyses of a *VAL1-GUS* translational fusion. (C) Expression in whole plants, scale bars = 1mm. (D) Expression in shoot apices following wax sectioning, scale bars = 0.1mm. (E, F) VAL1 levels quantified by MUG assay in two independent homozygous T3 lines. (A, B, E, F) Each data point represents a biological replicate and is the average of three technical replicates. Lines represent the mean and grey bars mean±s.e.m. Asterisks represent significant differences between two continuous time points, calculated by an unpaired two-tailed *t*-test (* $P < 0.05$; ** $P < 0.01$). All plants except the 3 DAG sample (C – long days) were grown in SD conditions.

479 3.8kb *VAL1* genomic sequence upstream of *GUS* in this construct (*VAL1::VAL1-GUS-*
480 *VAL1 3'UTR*). Because the expression of the transcriptional fusion was consistently
481 more diffuse, variable, and weaker than the expression of the translational fusion
482 (Supplementary file 6), we used plants containing the translational fusion for
483 subsequent studies.

484 During embryogenesis, the translational fusion was expressed in the root and
485 shoot apical meristems and provasculature (Figure 6C, Supplementary file 6). Following
486 germination, expression became restricted to the shoot and root apices and initiating
487 lateral root primordia (Figure 6C, Supplementary file 6). Throughout the rest of shoot
488 development, the translational fusion was expressed in the shoot apex and during the
489 early stages of leaf development (Figure 6C). Histological inspection indicated that
490 *VAL1* expression increases in the shoot apex during vegetative development. This was
491 validated by a quantitative analysis of GUS expression, which demonstrated that VAL1
492 accumulates more strongly in the shoot apex than leaf primordia. Further, that VAL1
493 levels increase over time in the shoot apex but not in older leaf primordia (Figure 6E,F).
494 Taken together, these data indicate that *VAL1* expression is restricted to apical
495 meristems and the early stages of root and leaf development. Our data also indicate
496 that *VAL1* expression increases during shoot development in very young leaf primordia,
497 quickly declines to a uniform level as the leaf develops, and ceases before the leaf is
498 fully expanded. However, the functional significance of increased VAL1 accumulation
499 during vegetative development is unclear, as we did not detect a concomitant increase
500 in VAL1-binding to *MIR156A/C* (Figure 4B, Supplementary file 3). Finally, the difference
501 in the staining patterns and stability of our transcriptional and translational reporters

502 suggest that *cis*-regulatory elements within the *VAL1* coding sequence regulate the
503 level and site of its expression.

504 VAL1 has previously been found to physically interact with VAL2, multiple PRC1
505 and PRC2 components, and the transcriptional repressor SAP18 (Chen et al., 2018,
506 2020; Chhun et al., 2016; Jing et al., 2019; Qüesta et al., 2016; Xie et al., 2018; Yang et
507 al., 2013a; Yuan et al., 2016). However, these studies do not provide information about
508 VAL1's *in planta* protein interactions over time. To determine whether VAL1 interacts
509 with different proteins at different stages of vegetative development, we carried out a
510 mass spectrometry analysis of proteins bound to HA-tagged VAL1 at 1, 2 and 3 weeks
511 of growth. Immunoprecipitations were carried out on a *VAL1-HA; val1-2; FRI-Sf2* line,
512 using a *val1-2; fri* line as a control. The difference in the *FRI* genotype of these lines is a
513 consequence of the genotypes available at the time the experiments were performed
514 and may have had an effect on our results.

515 ATBMI1A was significantly enriched in the combined experimental samples
516 relative to the control samples (Figure 7A), which is consistent with a previous mass
517 spectrometry analysis of proteins bound to VAL1-HA (Qüesta et al., 2016). We did not
518 detect other proteins that have been identified by mass spectrometry in
519 immunoprecipitation experiments with VAL1-HA. We also observed a highly significant
520 enrichment of the chloroplast binding protein CRB. However, this is explained by the
521 enrichment of CRB in the total proteome of the experimental versus control samples
522 (Figure 7B). Comparisons of the proteins present in samples harvested from 1, 2 and 3
523 weeks old plants revealed that ATBMI1A was consistently among the most abundant
524 proteins immunoprecipitated with VAL1-HA (Figure 7C-E). The abundance of ATBMI1A

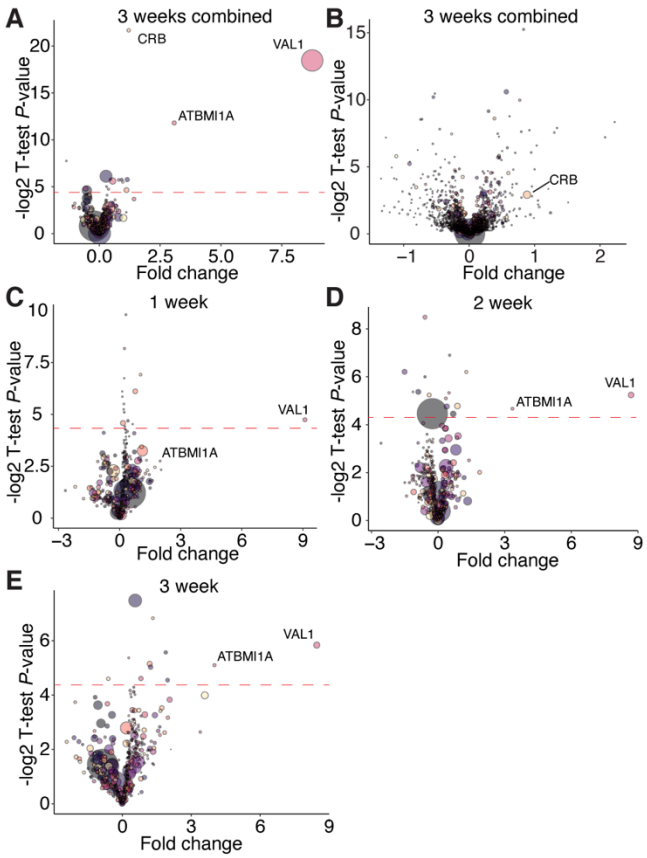

Figure 7. VAL1-protein interactions are consistent during vegetative development

(A-E) Protein enrichment calculated via mass spectrometry. Fold change represents the ratio of proteins purified from experimental (*VAL1-HA; val1-2; FRI-Sf2*) to control (*val1-2; fri*) samples, a t-test *P*-value is represented on the y-axis. Red dotted line indicates a *P*-value < 0.05 (resulting from the -log2 transformation of the actual p-value; proteins above the line have a significant enrichment). Each bubble represents an individual protein, the size or the bubble represents the protein abundance averaged across the experimental and control samples. (A, C-E) Proteins immunoprecipitated using an anti-HA antibody, (B) total proteome samples.

538 in the immunoprecipitated sample increased significantly from 1 week to 2 weeks, as
539 indicated by both the increase in the fold change between experimental and control
540 samples, and the statistical significance of the enrichment. This is probably a result of
541 the increase in the abundance of VAL1 between 1 and 2 weeks (Figure 6D,E), a result
542 which was confirmed by the increasing abundance of VAL1 in the immunoprecipitated
543 samples from different time points (Figure 7C-E). The parallel changes in the
544 abundance of VAL1-HA and ATBMI1A, and the absence of any major change in the
545 proteins associated with VAL1-HA in different samples, suggest that the binding
546 partners of VAL1 do not change significantly during shoot development.
547 To investigate overall trends in protein accumulation during vegetative
548 development we conducted a supervised clustering analysis of the *val1-2; VAL1-HA;*
549 *FRI-Sf2* total proteome sample. We designed two clusters in which proteins either
550 increased or decreased from 1 to 2 to 3 weeks of development (see Methods for
551 details). The 50 proteins with the strongest and most consistent decreasing
552 developmental trend were significantly enriched for Gene Ontology terms related to
553 photosynthesis and carbon fixation (Supplementary file 7). In contrast, the 50 proteins
554 with the highest increasing trend score were enriched for GO terms relating to water
555 stress and translation. The finding that younger plants invest more resources in
556 photosynthesis is consistent with a transcriptomic analysis of vegetative development in
557 maize (Beydler et al., 2016), and the enhanced photosynthetic capacity of juvenile
558 plants at low light levels (Lawrence et al., 2020).
559
560 **Discussion**

561 Plant life cycles are characterized by transitions between distinct developmental
562 phases. *VAL* genes have previously been shown to promote the switch from
563 embryogenesis to seed maturation (Suzuki et al., 2007; Yang et al., 2013a), and from
564 vegetative to reproductive growth (Qüesta et al., 2016; Yuan et al., 2016). The results
565 presented here demonstrate that *VAL1* and *VAL2* also regulate the intervening
566 transition from juvenile to adult stages of vegetative growth. *VAL* genes thus function as
567 a regulatory hub that coordinates developmental transitions throughout plant life cycles.
568
569 Regulation of miR156 expression by *VAL1/2*
570 Vegetative phase change is promoted by a temporal decline in miR156/miR157
571 expression (Wu and Poethig, 2006). When the level of miR156/miR157 falls below a
572 specific threshold, the de-repression of *SPL* genes initiates a switch to adult identity.
573 Previous work has shown that – with the exception of *SPL3* – the increase in *SPL*
574 transcript levels during development is entirely attributable to post-transcriptional
575 regulation by miR156/miR157 (He et al., 2018). Factors that control the timing of
576 vegetative phase change can therefore act in three ways: 1) by modifying the rate of
577 decline in miR156; 2) by constitutively increasing or decreasing the level of miR156; and
578 3) by constitutively increasing or decreasing the rate of transcription of *SPL* genes. Our
579 results suggest that *VAL1* and *VAL2* regulate vegetative phase change both by
580 constitutively decreasing the level of miR156 and by repressing *SPL* gene expression
581 independently of miR156.
582 Evidence that *VAL1/VAL2* constitutively regulate the level of miR156 was
583 provided by the phenotype of plants deficient for *VAL1* and *VAL2*, VAL1-DNA binding

584 patterns and from the phenotype of plants expressing a *MIR156C* transgene lacking
585 VAL-binding sites. We found that although *VAL1* expression increases in the shoot apex
586 as plants develop, *val1; val2* double mutants displayed only a slight decrease in the rate
587 at which miR156 declines. Instead, *val1; val2* double mutants exhibited a significant
588 increase in the level of miR156 at every stage of vegetative development we examined.
589 Consistent with this result, *mir156a; mir157a; mir157c* triple mutants transformed with a
590 *MIR156C* transgene lacking VAL-binding sites had elevated levels of miR156 relative to
591 the wild type *MIR156C* control, but displayed the same temporal decrease in miR156 as
592 control plants.

593 We have proposed that the decrease in *MIR156A/C* expression during shoot
594 development may be attributable to the stochastic replacement of H3K27ac and
595 H3K4me3 by H3K27me3 (Xu et al., 2018, 2016b). The observation that the increase in
596 miR156 expression in *val1; val2* is associated with a decrease in the level of H3K27me3
597 at *MIR156C* supports this hypothesis, in that it shows that H3K27me3 is associated with
598 low levels of *MIR156C* expression. The difference in the phenotype of plants doubly
599 mutant for *val1-2* and mutations the PRC2 histone methyltransferases, *SWN* and *CLF*,
600 and between *val1-2* and a mutation in the histone deacetylase *HDA19*, supports the
601 hypothesis that the expression of *MIR156C* is regulated by a combination of histone
602 marks. *val1-2; swn-3* and *val1-2; clf-29* double mutants have approximately the same
603 amount of miR156 as *val1-2* single mutants, which is expected given that these genes
604 are involved in the same process, namely the deposition of H3K27me3. In contrast,
605 *hda19-3* significantly enhanced the level of miR156 compared to *val1-2*. This type of

606 genetic interaction is predicted if miR156 expression is dependent on histone
607 modifications aside from H3K27me3.
608 The evidence that *VAL1/VAL2* regulate the level, but not the temporal expression
609 pattern, of miR156 leaves open the question of how its temporal pattern arises. Several
610 other chromatin regulators, such as the CHD3 nucleosome remodeler PICKLE (Xu et
611 al., 2016b), the PRC-accessory protein LHP1 (Cui et al., 2020), the SWI/SNF2
612 chromatin remodeler BRAHMA (Xu et al., 2016c), and the histone 2 regulators ARP6
613 and HTA9/11 (Choi et al., 2016; Xu et al., 2018) have been found to play a role in the
614 expression of miR156. Furthermore, transcription factors including AGL15/18
615 (Serivichyaswat et al., 2015), MYB33 (Guo et al., 2017), and members of the *NF-Y*
616 family (Wei et al., 2017; Zhao et al., 2020), also regulate miR156 expression. It is
617 possible that the temporal expression pattern of miR156 is a consequence of complex
618 interactions between these diverse factors, rather than being dependent on a single
619 class of regulator, such as *VAL1/2*.
620
621 <u>*VAL* genes and PRC1 activity</u>
622 *VAL1/2* are thought to be necessary for the recruitment of PRC1 to target loci,
623 where it represses gene expression via PRC2-dependent and independent mechanisms
624 (Baile et al., 2020; Yuan et al., 2020; Zhou et al., 2017). We found that *VAL1/2*
625 accelerate vegetative phase change by repressing the expression of *MIR156A/C*, and
626 by indirectly promoting the expression of *SPL9*, a target of miR156. These results are
627 consistent with a previous study (Pico et al., 2015), which showed that *VAL1/2* and the
628 PRC1 components, AtBMI1A/B, repress *MIR156A/C* expression. However, the PRC1

629 components EMBRYONIC FLOWER1 (Pico et al., 2015) and RING1A/B (Li et al., 2017)
630 have also been reported to repress the expression of *SPL9* independently of miR156.
631 These latter effects delay vegetative phase change, which is the exact opposite of the
632 effect produced by PRC1-mediated repression of *MIR156A/C*. Together, these results
633 indicate that PRC1 can operate at different points within a regulatory pathway, or in
634 interacting regulatory pathways, to modulate the output of the pathway or pathways. If
635 the genes repressed by PRC1 have different functions—as in the case of miR156 and
636 its *SPL* targets—then the functional significance of a particular level of PRC1 activity at
637 a particular locus can be difficult to predict. These results also support the hypothesis
638 that there may be different forms of PRC1, which target different genes. Moreover, our
639 finding that H2AK119ub deposition at *SPL9* was unaffected in *val1-5(sd); val2-3*
640 suggests that VAL1/2 may not be universally required for PRC1-recruitment.
641 In this regard, it is interesting that although *MIR156A* and *MIR156C* are close
642 paralogs and have similar expression patterns, previous studies (Xu et al., 2018,
643 2016b), and the results presented here, indicate that these genes are differentially
644 sensitive to mutations that affect the activity of PRC2 and PRC1. For example, we found
645 that *val1; val2* mutants display a greater reduction in H2AK119ub and H3K27me3 at
646 *MIR156C* than at *MIR156A*. Our findings align with the results of ChIP-seq studies of
647 H2AK119ub and H3K27me3 in *atbmi1a/b/c* (Zhou et al., 2017) and *val1-2; val2-3* (Yuan
648 et al., 2020) mutants. The implication of these observations is that *MIR156C* expression
649 is more dependent on PRC1 and PRC2 activity than *MIR156A.* Defining the molecular
650 basis for this difference could provide important insights into factors that influence
651 epigenetic regulation in plants.

652 Unlike in animals, where PRC1 binding requires the prior deposition of
653 H3K27me3, in plants PRC1 is thought to promote PRC2 activity at the majority of its
654 targets (Calonje, 2014; Zhou et al., 2017). This model is supported by our results. In the
655 case of *MIR156C*, we found that in 1 week old plants loss of *VAL1/2* significantly
656 reduced H2AK119ub, but not H3K27me3. However, by 3 weeks both H2AK119ub and
657 H3K27me3 were reduced in *val1/2* mutants. These results suggest that VAL1/2 and, by
658 inference, PRC1 are present at *MIR156C* prior to PRC2, and promote the activity of
659 PRC2.
660 In addition to their roles in vegetative phase change, *VAL* genes regulate multiple
661 nodes of the flowering time (Jing et al., 2019; Qüesta et al., 2016; Yuan et al., 2016)
662 and seed development (Chen et al., 2018, 2020; Suzuki et al., 2007; Yang et al., 2013a)
663 networks. The co-option of *VAL* activity throughout genetic networks thus appears
664 critical to coordinating plant developmental transitions. Despite the centrality of *VAL*
665 function to the control of developmental timing, the persistent and robust pattern of
666 *MIR156A/C* expression in *val* mutant plants emphasizes the complexity of temporal
667 regulation in plants.
668

669 **Materials and methods**

670 **Plant material and growth conditions**

671 All stocks were grown in the Col-0 background. The following genetic lines have been
672 described previously: *val1-2* (SALK_088606)*, val2-1* (CS906036) (Suzuki et al., 2007)
673 (*val2-1* was backcrossed to Col-0 6 times from the original Wassilewskija parent); *val2-3*
674 (SALK_059568C) (Yang et al., 2013a); *clf-29* (SALK_021003) (Bouveret et al., 2006);

675 *swn-3* (SALK_050195) (Chanvivattana et al., 2004); *hda19-3* (SALK_139445) (Kim et
676 al., 2008); *mir156a-2 mir156c-1 mir157a-1 mir157c-1* (He et al., 2018); *SPL9::rSPL9-*
677 *GUS* (Xu et al., 2016a); *val1-2 VAL1::VAL1-3xHA FRI-Sf2* (Qüesta et al., 2016). *val2-4*
678 (SALK_127961) was obtained from the Arabidopsis Biological Resources Center (Ohio
679 State University, OH, USA). Seeds were sown on fertilized Farfard #2 soil (Farfard) and
680 kept at 4°C for 3 days prior to transfer to a growth chamber, with the transfer day
681 counted as day 0 for plant age (0 DAG – days after germination). Plant were grown at
682 22°C under a mix of both white (USHIO F32T8/741) and red-enriched (Interlectric
683 F32/T8/WS Gro-Lite) fluorescent bulbs in either long day (16 hrs light/8 hrs. dark; 40
684 µmol m^{-2} s^{-1}) or short day (10 hrs light/14 hrs dark; 100 µmol m^{-2} s^{-1}) conditions.
685

686 **Identification of the *val1-5(sd)* mutant**

687 The *val1-5(sd)* allele was generated by exposing *mir157a-1; mir157c-1* seed to ethyl
688 methanesulfonate. An M2 mutant plant exhibiting delayed vegetative phase change was
689 backcrossed to the parental line and allowed to self. Tissue was pooled from 30 plants
690 exhibiting severely delayed vegetative phase change in the BC1F2 generation. DNA
691 was extracted via-SDS lysis and phenol-chloroform extraction and further purified using
692 Clean and Concentrator columns (Zymo Research). DNA concentration was determined
693 using a Qubit 2.0 Fluorometer (Invitrogen) and 1µg of DNA sheared using a Covaris S2
694 sonicator (Covaris) to produce 350bp inserts. Sequencing libraries were made following
695 the TruSeq DNA PCR-free LT Sample Prep Kit (Illumina) manufacturer's instructions.
696 Library quality and quantity was validated by Bioanalyser (Agilent) and KAPA analysis
697 (Kapa Biosystems). 100bp paired end reads were generated using a HiSeq 2500

698 (Illumina) and aligned to the TAIR10 reference genome following the default SHORE
699 pipeline (Ossowski et al., 2008). The SHOREmap backcross pipeline (Schneeberger et
700 al., 2009) using default options was employed to identify polymorphisms. Manual
701 inspection of allele frequencies in the mutant revealed a peak centered on the *VAL1*
702 locus. The causative mutation was confirmed by Sanger sequencing and
703 complementation assays. The mutant was backcrossed to a 'Traffic Line' (Wu et al.,
704 2015) with seed-fluorescent markers inserted adjacent to the *VAL1* locus to eliminate
705 additional closely linked polymorphisms. Consequently, the resultant *val1-5(sd)* plants
706 used in this study contain a linked *pNAP::RFP* insertion at 13,622,737bp on
707 Chromosome 2 (Crick strand).
708
709 **Generation of transgenic plants**
710 For RY-mutation lines the RY-site TGCATG was replaced by TGTATG. A 5kb *MIR156C*
711 genomic sequence including 2kb upstream of the transcriptional start site and 665bp
712 downstream of the end of the last exon was cloned into the binary vector pAGM4723
713 from the Golden Gate MoClo toolbox supplied by Addgene (www.addgene.org) (Weber
714 et al., 2011; Werner et al., 2012). For -RY3, -RY4 and -RY5 Q5 Site Directed
715 Mutagenesis Kit (New England Biolabs) was used to induce a substitution directly into
716 the expression vector. For -RY1, -RY2 and -RY12345 Gibson Assembly cloning (New
717 England Biolabs) was used to assemble individual fragments into the same backbone.
718 Golden Gate cloning was also used to generate *VAL1::VAL1-VAL1 3'UTR*,
719 *VAL1::VAL1-GUS-VAL1 3'UTR*, *VAL1::GUS-VAL1 3'UTR* lines. Promoter/5'UTR (*VAL1*

720 - 2.3kb), functional (*VAL1* – 3.8kb, *MIR156A* (Fouracre and Poethig, 2019)) and
721 3'UTR/terminator (*VAL1* – 2kb) sequences were cloned separately from *Arabidopsis*
722 gDNA, with Type II restriction sites removed where necessary. *GUS* and *AtuOCS*
723 sequences were obtained from the MoClo Plant Parts toolkit supplied by Addgene
724 (www.addgene.org) (Engler et al., 2014). Component parts were assembled using
725 Golden Gate cloning into the pAGM4723 binary vector, including green or red seed
726 fluorescent expression cassettes as selectable markers. Constructs were transformed
727 into *Arabidopsis* using the floral dip method. All primers used for cloning are included in
728 Supplementary table 1.
729
730 **Quantification of gene expression**
731 Tissue (either shoot apices with leaf primordia ≤1mm attached or isolated leaf primordia
732 0.5-1mm in size – as specified in the text) were ground in liquid nitrogen and total RNA
733 extracted using Trizol (Invitrogen) as per the manufacturer's instructions. RNA was
734 treated with RNAse-free DNAse (Qiagen) and 250ng-1µg of RNA was used for reverse
735 transcription using Superscript III (Invitrogen). Gene specific RT primers were used to
736 amplify miR156, miR157, miR172 and SnoR101 and a polyT primer for mRNA
737 amplification. Three-step qPCR of cDNA was carried out using SYBR-Green Master Mix
738 (Bimake). qPCR reactions were run in triplicate and an average was calculated.
739 Relative transcript levels were normalized to snoR101 (for miRNAs) and *ACT2* (for
740 mRNAs) and expressed as a ratio of expression to a specified control sample. The
741 qPCR primers used in this study are listed in Supplementary table 1.
742

743 **Chromatin immunoprecipitation**

744 Expanded leaves and roots were removed during tissue harvesting to produce samples
745 enriched for shoot apices and young leaves. For histone ChIP ~0.5g of fresh tissue per
746 antibody and for anti-HA ChIP ~5g of fresh tissue were harvested. Samples were fixed
747 in 1% formaldehyde under vacuum for 15 minutes. Cross-linked samples were ground
748 in liquid nitrogen and suspended in Honda buffer (0.44M sucrose, 1.25% ficoll, 2.5%
749 dextran 40, 20mM hepes pH 7.4, 10mM $MgCl_2$, 0.5% Triton, 5mM DTT, 1mM PMSF,
750 1% protease inhibitors), filtered through two layers of Miracloth (EMD Millipore), and
751 pelleted and washed thrice in Honda buffer. For histone ChIP, pellets were
752 resuspended in nuclei lysis buffer (50mM Tris-HCl pH 8, 10mM EDTA, 1% SDS, 1%
753 protease inhibitors), for anti-HA ChIP, pellets were resuspended in RIPA buffer (1X
754 PBS, 1% NP-40, 0.5% sodium deoxycholate, 0.1% SDS, 1% protease inhibitors).
755 Samples were sonicated using a Fisherbrand Sonic Dismembrator (Fisher Scientific) 6x
756 10s at setting 3.2. ChIP samples were pre-cleared using Dynabeads Protein A
757 (Invitrogen). 2% was removed as input and samples were incubated overnight with 1%
758 antibody (for histone ChIP: anti-H3 (abcam ab1791), anti-H3K27me3 (EMD Millipore 07-
759 449), anti-H2AK119ub (Cell Signaling Technology 8240); for VAL1-HA ChIP: anti-HA
760 (Roche 11583816001)). Chromatin-antibody conjugates were purified with Dynabeads
761 Protein A and washed in low/high salt, lithium and TE buffers. Following reverse-
762 crosslinking DNA was isolated using a QIAquick PCR Purification Kit (Qiagen).

763 For ChIP-qPCR assays, three-step qPCR was carried out using SYBR-Green
764 Master Mix (Bimake). qPCR reactions were run in triplicate and an average was
765 calculated. Data were normalized and presented as follows: 1) For H3K27me3 – *STM*

766 was used as a control locus, data is presented as a ratio of (H3K27me3 gene of
767 interest/H3 gene of interest) to (H3K27me3 *STM*/H3 *STM*); 2) For H2AK119ub – *ACT7*
768 was used as a control locus, data is presented as a ratio of (H2AK119ub gene of
769 interest/input gene of interest) to (H2AK119ub *ACT7*/input *ACT7*); 3) For VAL1-HA –
770 *UBQ10, ACT7* and *TA3* were used as control loci, data is presented as a ratio of
771 ((VAL1-HA ChIP gene of interest/input gene of interest)/(VAL1-HA ChIP control/input
772 control)) relative to ((WT ChIP gene of interest/input gene of interest)/(WT ChIP
773 control/input control)). The qPCR primers used in this study are listed in Supplementary
774 table 1.
775
776 **Mass spectrometry**
777 *VAL1::VAL1-3xHA; val1-2; FRI-Sf2* and *val1-2* genotypes were used as experimental
778 and control samples respectively. Expanded leaves and roots were removed during
779 tissue harvesting to produce samples enriched for shoot apices and young leaves. 2-3g
780 of fresh tissue was harvested for immunoprecipitation, 0.2-0.6g was harvested for total
781 protein extraction. For immunoprecipitation, tissue was ground in liquid nitrogen,
782 suspended in IP buffer (20mM Tris-HCl pH 8, 150mM NaCl, 2.5mM EDTA, 0.5% Triton,
783 1% protease inhibitors, 1mM PMSF), rotated for 2 hours at 4°C and filtered through 2
784 layers of Miracloth. Anti-HA (Roche) conjugated Dynabeads Protein A (Invitrogen) were
785 added and samples were rotated overnight at 4°C. Beads were washed thrice with IP
786 buffer and proteins were purified for mass spectrometry using an S-Trap: Rapid
787 Universal MS Sample Prep (Protifi) following the manufacturer's instructions. For total
788 proteomes, ground tissue was suspended in 8M urea and rotated at room temperature

789 for 45 minutes. The samples were centrifuged thrice and the supernatant reduced with
790 DTT (final concentration 5mM) and alkylated with iodoacetamide 40 (final concentration
791 40mM) before overnight digest with trypsin. Samples were resuspended in 10 µl of
792 water + 0.1% TFA and loaded onto a Dionex RSLC Ultimate 300 (Thermo Scientific,
793 San Jose, CA, USA), coupled online with an Orbitrap Fusion Lumos (Thermo Scientific).
794 Chromatographic separation was performed with a two-column system, consisting of a
795 C_{18} trap cartridge (300 µm ID, 5 mm length) and a picofrit analytical column (75 µm ID,
796 25 cm length) packed in-house with reversed-phase Repro-Sil Pur C_{18}-AQ 3 µm resin.
797 Peptides were separated using a 90 min gradient (for the IP experiments) and 180 min
798 (for the full proteome experiment) from 2-28% buffer-B (buffer-A: 0.1% formic acid,
799 buffer-B: 80% acetonitrile + 0.1% formic acid) at a flow rate of 300 nl/min. The mass
800 spectrometer was set to acquire spectra in a data-dependent acquisition (DDA) mode.
801 Briefly, the full MS scan was set to 300-1200 m/z in the orbitrap with a resolution of
802 120,000 (at 200 m/z) and an AGC target of 5x10e5. MS/MS was performed in the ion
803 trap using the top speed mode (2 secs), an AGC target of 10e4 and an HCD collision
804 energy of 30. Raw files were searched using Proteome Discoverer software (v2.4,
805 Thermo Scientific) using SEQUEST as search engine using the SwissProt *Arabidopsis*
806 *thaliana* database. The search for total proteome included variable modifications of
807 methionine oxidation and N-terminal acetylation, and fixed modification of
808 carbamidomethyl cysteine. Trypsin was specified as the digestive enzyme. Mass
809 tolerance was set to 10 pm for precursor ions and 0.2 Da for product ions. Peptide and
810 protein false discovery rate was set to 1%. Data transformation, normalization and

811 statistical analysis using heteroscedastic t-test was performed as previously described
812 (Aguilan et al., 2020).
813 Proteins were sorted according to their descending or ascending linearity across
814 the three weeks. To do so, we used a custom score taking into account monotonic
815 trend, reproducibility across replicates and magnitude of change across weeks. The 50
816 proteins with the highest descending and ascending trend scores were used to identify
817 enriched GO terms for biological processes using the Fisher's Exact PANTHER
818 Overrepresentation Test (released 2020-07-28) and GO Ontology database DOI:
819 10.5281/zenodo.4081749 (released 2020-10-09). The *Arabidopsis thaliana* genome
820 was used as a reference list. Protein interaction maps for the same sets of 50 proteins
821 were made using the STRING app from Cytoscape (Shannon et al., 2003).
822
823 **GUS staining and histology**
824 Shoot apices and whole plants were fixed in 90% acetone on ice for 10 minutes,
825 washed with GUS staining buffer (5mM potassium ferricyanide and 5mM ferrocyanide in
826 0.1M PO_4 buffer) and incubated at 37°C overnight in GUS staining buffer with 2mM X-
827 Gluc. Embryos were placed directly in X-Gluc (GoldBio) GUS staining buffer and
828 incubated for 1hr. To quantify GUS activity, a 4-methylumbelliferyl b-D-glucuronide
829 (MUG) (Sigma-Aldrich) assay was carried out as previously described (He et al., 2018).
830 For histological observations individuals were fixed in FAA (3.7% formaldehyde),
831 dehydrated in an ethanol series and cleared using Histo-Clear (National Diagnostics).
832 Following embedding in Paraplast Plus (Sigma-Aldrich) 8μM sections were produced

833 using an HM 355 microtome (Microm) and visualized using an Olympus BX51
834 microscope with a DP71 camera attachment (Olympus).
835
836 **Quantification and statistical analyses**
837 Details of all statistical analyses, including the type of statistical test, sample size,
838 replicate number and significance threshold, are included in the relevant figure legend.
839 For figures featuring boxplots, boxes display the IQR (boxes), median (lines), and
840 values beyond 1.5* IQR (whiskers); mean values are marked by a solid diamond (◆).
841 Statistical analyses were carried out using RStudio (RStudio Team, 2020) and Microsoft
842 Excel. Measurements of leaf shape were made using ImageJ (Schindelin et al., 2012).
843
844 **Materials Availability**
845 The *val1-5(sd), val1-5(sd); val2-3*, *val1-2; val2-4, val1-2; mir156ac mir157ac* and
846 *VAL1::VAL1-GUS-VAL1 3'UTR* lines described herein have been donated to the ABRC
847 (stock numbers CS72451-CS72455 respectively). All other plant lines and plasmids
848 generated during this project are available on request to Scott Poethig
849 (spoethig@sas.upenn.edu).
850
851 **Acknowledgements**
852 We thank members of the R.S.P laboratory and Doris Wagner (University of
853 Pennsylvania) for helpful discussions, Daniel Martinez and Ryan McCarthy (University
854 of Pennsylvania) for assistance with histology and chromatin sonication, the Arabidopsis
855 Biological Resource Center for T-DNA insertion lines and Julia Qüesta and Caroline

Dean (John Innes Center) for the kind donation of *VAL1-HA; val1-2; FRI-Sf2* seed. This project was funded by NIH Grant GM051893 (to R.S.P). S.S. gratefully acknowledges Merck/MSD for the Umberto Mortari Award (2019), the Japan Agency for Medical Research and Development (AMED) and the New York Academy of Sciences (NYAS) for supporting aging research in his lab.

Author Contributions

Conceptualization: J.P.F., R.S.P.; Methodology: J.P.F., R.S.P.; Investigation: J.P.F., J.H., V.J.C., S.S.; Formal analysis: J.P.F., S.S.; Resources: J.P.F., J.H.; Visualization: J.P.F., S.S.; Writing - original draft: J.P.F.; Writing - review & editing: J.P.F., J.H., S.S., R.S.P.; Supervision: R.S.P.; Project administration: R.S.P.; Funding acquisition: R.S.P.

Declaration of Interests

The authors declare no competing interests.

Supplemental files titles and legends

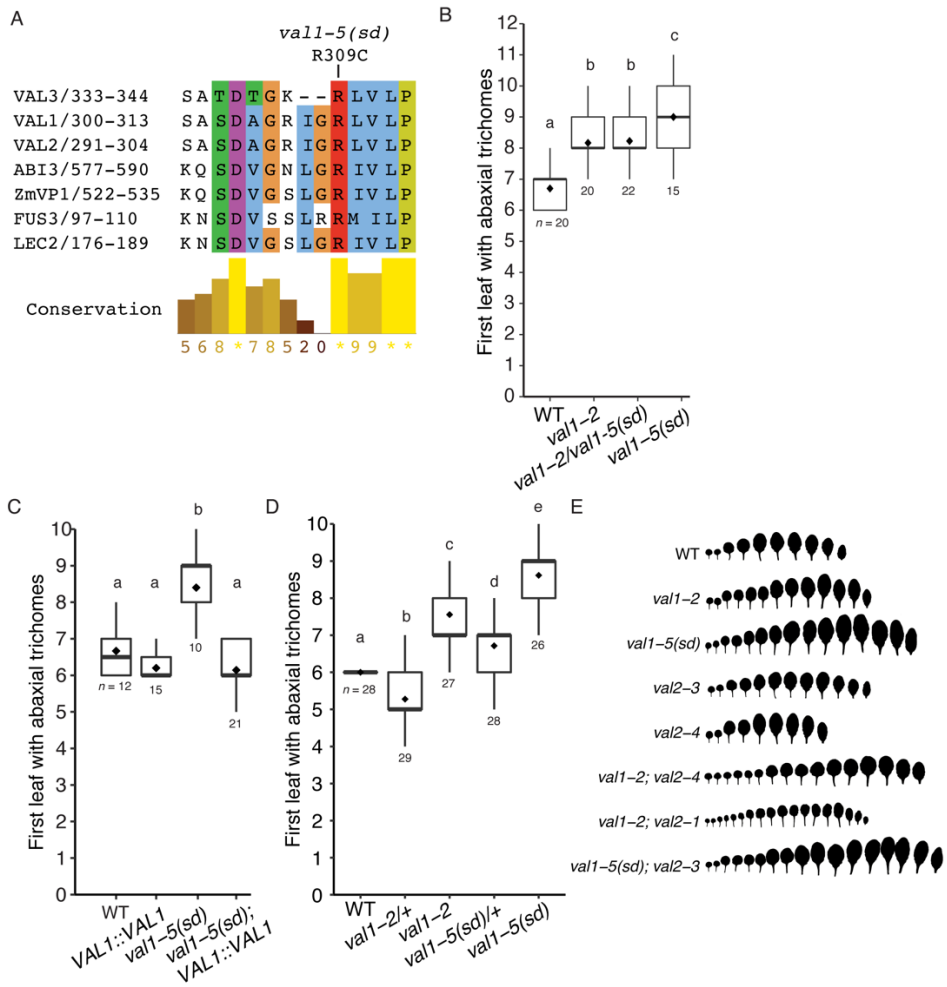

Supplementary file 1. *val1-5(sd)* is an antimorphic allele

(A) Sequence alignment of the B3 DNA-binding domain N-arm of *Arabidopsis* LAV family members and the maize ABI3 ortholog VP1. Numbers correspond to amino acid sequence numbers, colors correspond to the ClustalX amino acid color scheme. In the *val1-5(sd)* mutant a C>T base substitution converts an arginine to a cysteine.

(B) *val1-5(sd)* complementation test with the null *val1-2* allele

(C) Rescue of the *val1-5(sd)* abaxial trichome phenotype with a *VAL1* genomic sequence. Independent T1 lines are shown.

884 (D) Allele heterozygosity testing. (B-D) Boxes display the interquartile range (IQR)
885 (boxes), median (lines) and values beyond 1.5*IQR (whiskers); mean values are
886 marked by ◆. Samples sizes are displayed on the graph. Statistically distinct
887 genotypes were identified by one-way ANOVA with *post hoc* Tukey multiple
888 comparison test (letters indicate statistically distinct groups; $P < 0.05$), all plants
889 grown in LD.
890 (E) Heteroblastic series of lines shown in Figure 1.
891

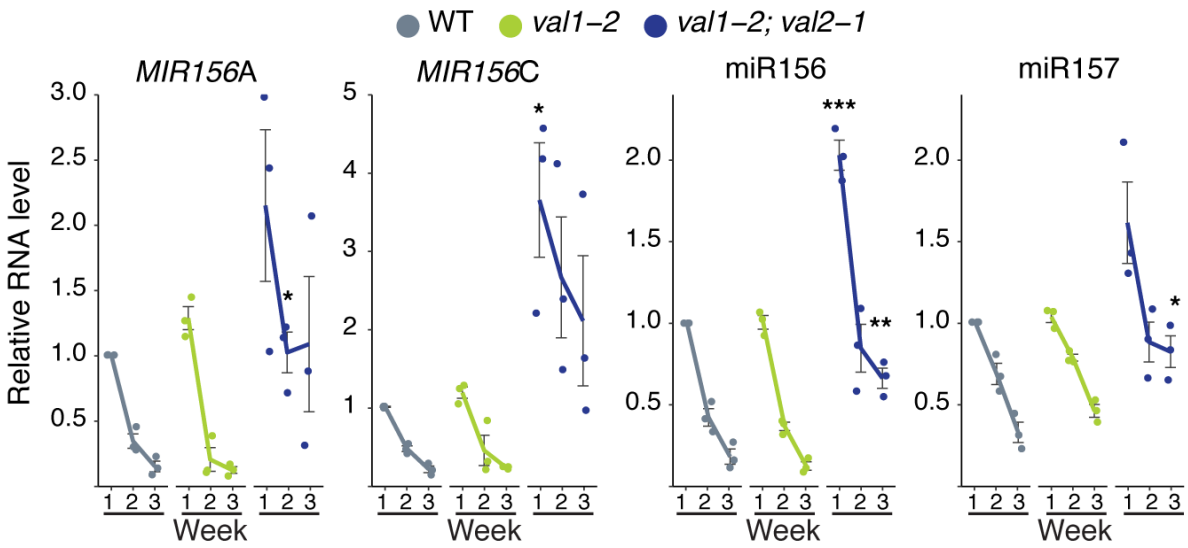

892

893 **Supplementary file 2. *VAL* genes redundantly regulate miR156 expression**

894 qRT-PCR analyses of gene expression in shoot apices with leaf primordia (LP) ≥
895 1mm removed at 1, 2 and 3 weeks. All plants were grown in SD conditions. Each
896 data point represents a biological replicate and is the average of three technical
897 replicates. Coloured lines represent the mean and black lines mean±s.e.m.
898 Asterisks represent significant differences between WT and *val* mutants at the
899 same time point, calculated by an unpaired two-tailed *t*-test with a Bonferroni
900 correction for multiple comparisons (* $P < 0.025$; ** $P < 0.005$; *** $P < 0.0005$).

901

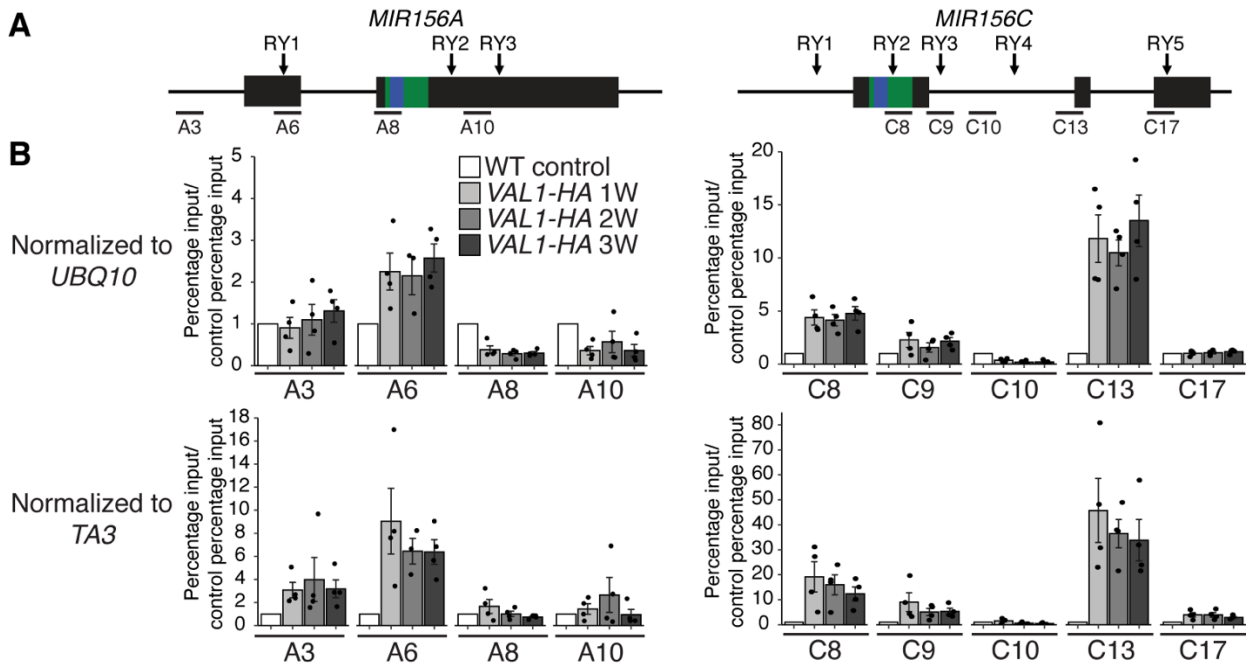

Supplementary file 3. VAL1 binds consistently to *MIR156A* and *MIR156C* during vegetative development

(A) Schematic depicting the location of primers used for ChIP-qPCR, the sequences encoding the miR156 hairpin and mature miRNA are coloured green and blue respectively.

(B) Anti-HA ChIP-qPCR of WT Col control plants at 2W and *VAL1::VAL1-HA; val1-2; FRI-Sf2* plants at 1, 2 and 3W of growth. The data is presented as percentage input normalized to a control locus (*UBQ10* or *TA3*) and is displayed relative to WT. Each data point represents a biological replicate and is the average of three technical replicates, bars represent the mean and error bars the mean±s.e.m. Plants were grown in SD conditions.

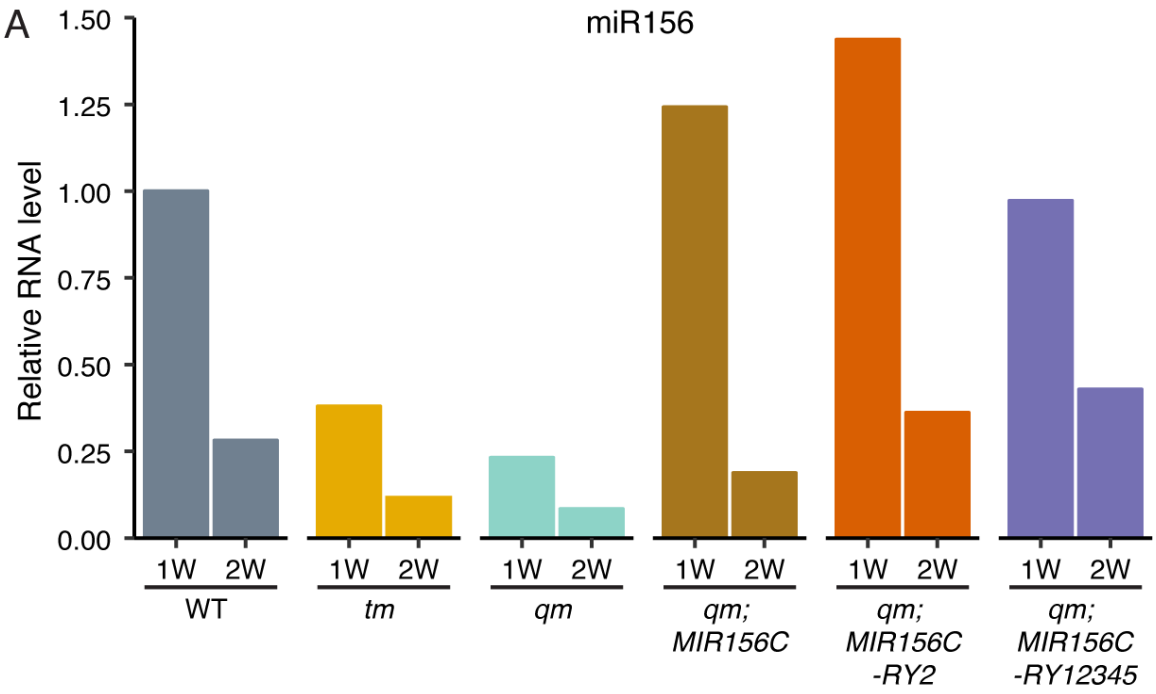

Supplementary file 4. RY sites are not required for the temporal decline of *MIR156C*

(A) qRT-PCR analyses of gene expression in shoot apices with LP ≥ 1mm removed at 1 and 2 weeks. Bars represent the average of three technical replicates for a single biological replicate of pooled T1 plants, at least 15 independent T1 plants were pooled for each sample. *qm = mir156a mir156c mir157a mir157c quadruple mutant, tm = mir156a mir157a mir157c triple mutant*. Plants were grown in SD conditions.

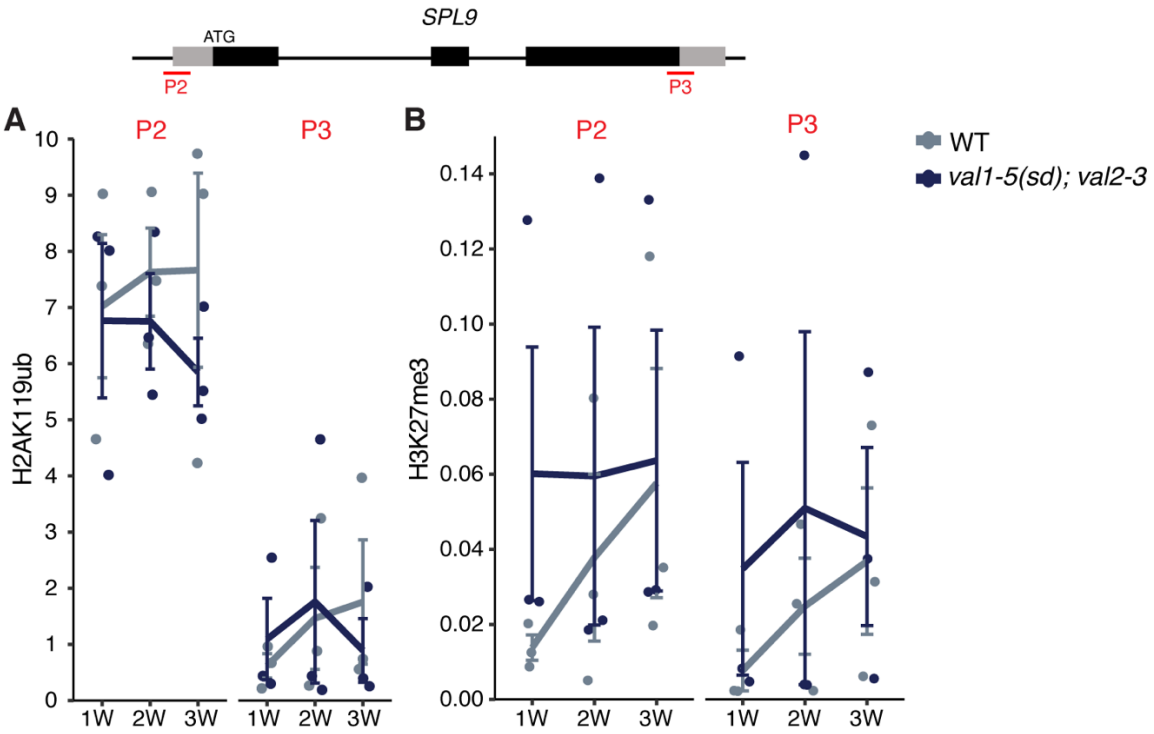

925

926 **Supplementary file 5. *VAL* genes do not regulate *SPL9* chromatin state**

927 (A, B) Temporal analysis of histone modification scalculated by ChIP-qPCR. Each data

928 point represents a biological replicate and is the average of three technical

929 replicates. Lines represent the mean and bars represent the mean±s.e.m., (A)

930 H3K2me3 values are relative to H3 and normalised to *STM* as an internal control.

931 (B) H2AK119ub values are relative to input and normalised to *ACT7* as an

932 internal control. Plants were grown in SD conditions.

933

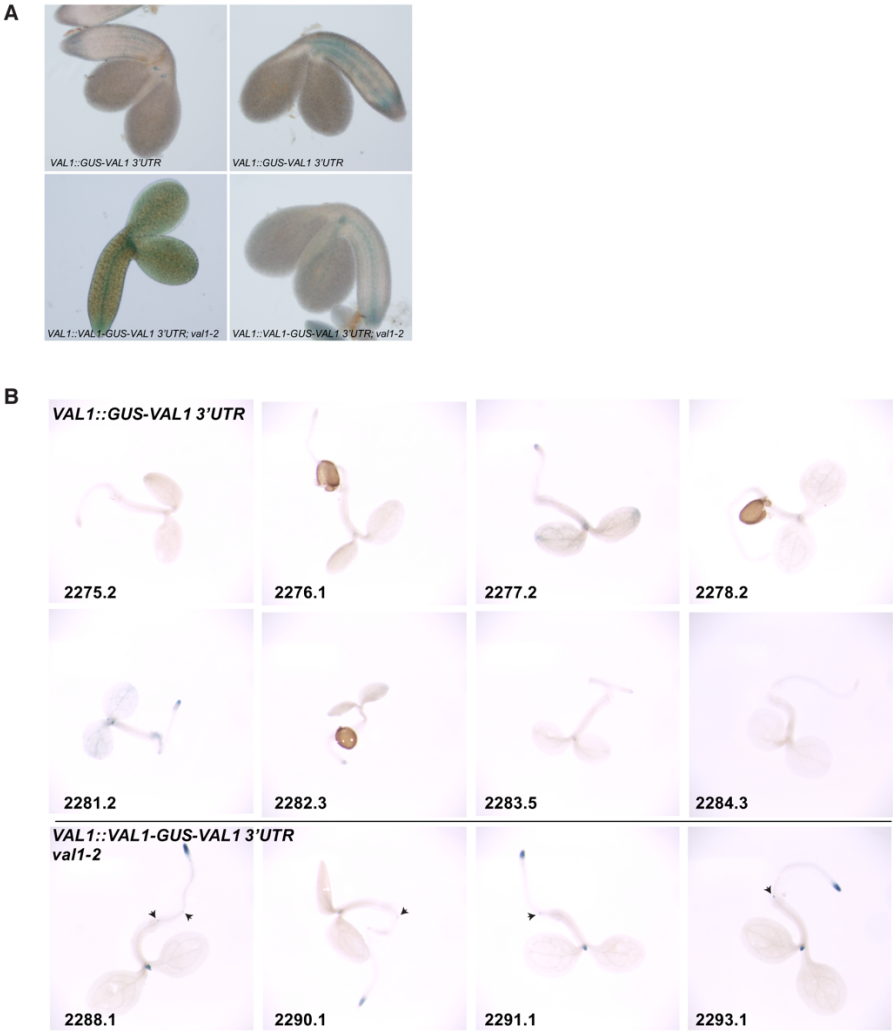

934

935 **Supplementary file 6. *VAL1* expression is dependent on genetic elements in the**

936 **coding sequence of the gene**

937 (A) Torpedo-stage embryos of two-independent homozygous transgenic lines each

938 expressing a transcriptional (top panel) or translational (bottom panel) *VAL1-*

939 *GUS* reporter construct.

940 (B) Seedlings at 3 DAG. Each number designates an independent homozygous

941 transgenic line. Arrow heads point to initiating lateral root primordia. All plants

942 were grown in LD.

943

A

Ascending Cluster			Descending Cluster		
GO Term	*P* value	FDR	GO Term	*P* value	FDR
response to cadmium ion (GO:0046686)	1.71E-14	5.12E-11	response to cold (GO:0009409)	2.81E-20	1.68E-16
response to cold (GO:0009409)	4.12E-09	3.08E-06	response to cadmium ion (GO:0046686)	4.90E-13	5.86E-10
response to water deprivation (GO:0009414)	4.18E-06	1.14E-03	reductive pentose-phosphate cycle (GO:0019253)	1.84E-10	7.34E-08
nucleocytoplasmic transport (GO:0006913)	5.19E-05	1.00E-02	defense response to bacterium (GO:0042742)	4.03E-09	1.10E-06
response to zinc ion (GO:0010043)	7.59E-05	1.26E-02	gluconeogenesis (GO:0006094)	1.64E-07	2.89E-05
ribosomal large subunit assembly (GO:0000027)	8.11E-05	1.31E-02	fructose 1,6-bisphosphate metabolic process (GO:0030388)	2.53E-06	3.29E-04
toxin catabolic process (GO:0009407)	9.81E-05	1.50E-02	response to sucrose (GO:0009744)	1.01E-05	1.02E-03
defense response to bacterium (GO:0042742)	1.10E-04	1.60E-02	pentose-phosphate shunt (GO:0006098)	3.87E-05	3.35E-03
positive regulation of protein-containing complex disassembly (GO:0043243)	1.16E-04	1.65E-02	response to light stimulus (GO:0009416)	4.30E-05	3.57E-03
unidimensional cell growth (GO:0009826)	1.87E-04	2.54E-02	ATP synthesis coupled proton transport (GO:0015986)	7.59E-05	5.90E-03
cellular response to hydrogen peroxide (GO:0070301)	2.49E-04	3.11E-02	ammonia assimilation cycle (GO:0019676)	9.00E-05	6.41E-03
response to abscisic acid (GO:0009737)	2.94E-04	3.59E-02	photosynthetic electron transport chain (GO:0009767)	9.22E-05	6.49E-03
translation (GO:0006412)	3.34E-04	3.70E-02	glycine decarboxylation via glycine cleavage system (GO:0019464)	1.16E-04	7.85E-03
			defense response to fungus, incompatible interaction (GO:0009817)	1.24E-04	8.07E-03
			carbon utilization (GO:0015976)	1.44E-04	9.28E-03
			glycolytic process (GO:0006096)	1.54E-04	9.51E-03
			protein folding (GO:0006457)	3.58E-04	1.96E-02
			plastid translation (GO:0032544)	7.31E-04	3.80E-02
			chloroplast organization (GO:0009658)	9.79E-04	4.96E-02

B

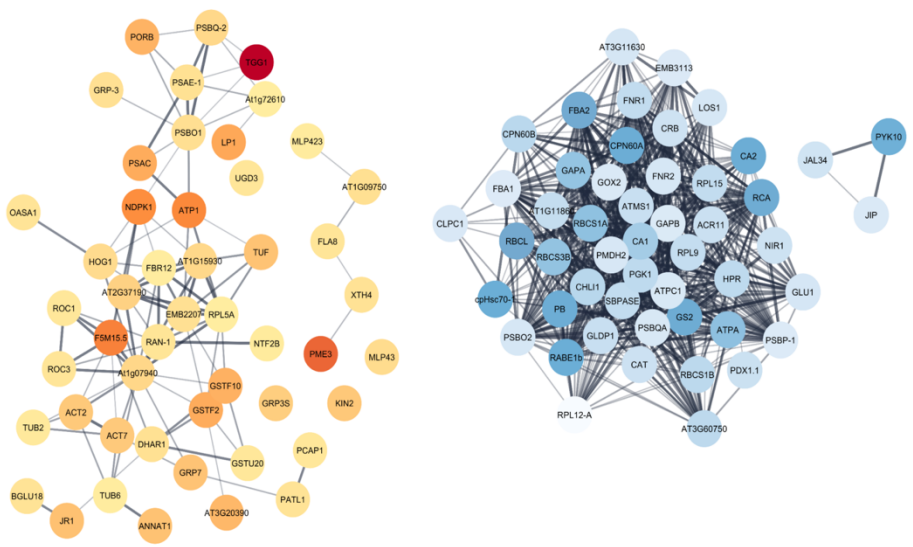

944

945 **Supplementary file 7. Proteomic changes during vegetative development**

946 (A,B) The 50 proteins with the strongest increasing or decreasing trend score during
947 vegetative development in the experimental sample only (see Methods for
948 details). (A) GO terms enriched within the 50 proteins that have the strongest
949 increasing or decreasing trend score. (G) Interaction networks for each set of 50
950 proteins, the darker the color the stronger the increasing (red) or decreasing
951 (blue) trend score.

952

953 **Supplementary table 1. Primer sequences**

954 This table includes all the primer sequences used in this study.

955

956 **Supplementary table 2. Proteins detected by mass spectrometry following anti-**

957 **HA immunoprecipitation**

958 Related to Supplementary file 6.

959 This table includes the raw mass spectrometry results and data processing for IP-

960 samples.

961

962 **Supplementary table 3. Total proteome changes during vegetative development**

963 Related to Supplementary file 6.

964 This table includes the raw mass spectrometry results and data processing for total

965 proteome samples.

966

967 **References**

968 Aguilan, J.T., Kulej, K., and Sidoli, S. (2020). Guide for protein fold change and p-value
969 calculation for non-experts in proteomics. Mol. Omics *16*, 573–582.

970 Baile, F., Merini, W., Hidalgo, I., and Calonje, M. (2020). Dissection of PRC1 and PRC2
971 recruitment in Arabidopsis connects EAR repressome to PRC2 anchoring. BioRxiv
972 2020.08.28.271999.

973 Beydler, B., Osadchuk, K., Cheng, C.-L., Manak, J.R., and Irish, E.E. (2016). The Juvenile Phase of
974 Maize Sees Upregulation of Stress-Response Genes and Is Extended by Exogenous Jasmonic
975 Acid. Plant Physiol. *171*, 2648–2658.

976 Bouveret, R., Schönrock, N., Gruissem, W., and Hennig, L. (2006). Regulation of flowering time
977 by *Arabidopsis MSI1*. Development *133*, 1693–1702.

978 Bratzel, F., López-Torrejón, G., Koch, M., Del Pozo, J.C., and Calonje, M. (2010). Keeping Cell
979 Identity in Arabidopsis Requires PRC1 RING-Finger Homologs that Catalyze H2A
980 Monoubiquitination. Current Biology *20*, 1853–1859.

981 Calonje, M. (2014). PRC1 Marks the Difference in Plant PcG Repression. Molecular Plant *7*, 459–
982 471.

983 Carbonero, P., Iglesias-Fernández, R., and Vicente-Carbajosa, J. (2017). The AFL subfamily of B3
984 transcription factors: evolution and function in angiosperm seeds. Journal of Experimental
985 Botany *68*, 871–880.

986 Chanvivattana, Y., Bishopp, A., Schubert, D., Stock, C., Moon, Y.-H., Sung, Z.R., and Goodrich, J.
987 (2004). Interaction of Polycomb-group proteins controlling flowering in *Arabidopsis*.
988 Development *131*, 5263–5276.

989 Chen, N., Veerappan, V., Abdelmageed, H., Kang, M., and Allen, R.D. (2018). HSI2/VAL1 Silences
990 *AGL15* to Regulate the Developmental Transition from Seed Maturation to Vegetative Growth
991 in Arabidopsis. Plant Cell *30*, 600–619.

992 Chen, N., Wang, H., Abdelmageed, H., Veerappan, V., Tadege, M., and Allen, R.D. (2020).
993 HSI2/VAL1 and HSL1/VAL2 function redundantly to repress DOG1 expression in Arabidopsis
994 seeds and seedlings. New Phytologist *227*, 840–856.

995 Chhun, T., Chong, S.Y., Park, B.S., Wong, E.C.C., Yin, J.-L., Kim, M., and Chua, N.-H. (2016). HSI2
996 Repressor Recruits MED13 and HDA6 to Down-Regulate Seed Maturation Gene Expression
997 Directly During Arabidopsis Early Seedling Growth. Plant and Cell Physiology *57*, 1689–1706.

998 Choi, K., Kim, J., Muller, S.Y., Oh, M., Underwood, C., Henderson, I., and Lee, I. (2016).
999 Regulation of microRNA-mediated developmental changes by the SWR1 chromatin remodeling
1000 complex. Plant Physiol *171*, 1128–1143.

1001 Cui, Y., Cheng, J., Ruan, S., Qi, P., Liu, W., Bian, H., Ye, L., Zhang, Y., Hu, J., Dong, G., et al. (2020).
1002 The heterochronic gene Oryza sativa LIKE HETEROCHROMATIN PROTEIN 1 modulates
1003 miR156b/c/i/e levels. Journal of Integrative Plant Biology *62*, 1839–1852.

1004 Engler, C., Youles, M., Gruetzner, R., Ehnert, T.M., Werner, S., Jones, J.D., Patron, N.J., and
1005 Marillonnet, S. (2014). A golden gate modular cloning toolbox for plants. ACS Synth. Biol. *3*,
1006 839–843.

1007 Fouracre, J.P., and Poethig, R.S. (2019). Role for the shoot apical meristem in the specification
1008 of juvenile leaf identity in *Arabidopsis*. Proc Natl Acad Sci USA *116*, 10168–10177.

1009 German, M.A., Pillay, M., Jeong, D.-H., Hetawal, A., Luo, S., Janardhanan, P., Kannan, V.,
1010 Rymarquis, L.A., Nobuta, K., German, R., et al. (2008). Global identification of microRNA–target
1011 RNA pairs by parallel analysis of RNA ends. Nature Biotechnology *26*, 941–946.

1012 Goodrich, J., Puangsomlee, P., Martin, M., Long, D., Meyerowitz, E.M., and Coupland, G. (1997).
1013 A Polycomb-group gene regulates homeotic gene expression in Arabidopsis. Nature *386*, 44–51.

1014 Gou, J.Y., Felippes, F.F., Liu, C.J., Weigel, D., and Wang, J.W. (2011). Negative regulation of
1015 anthocyanin biosynthesis in Arabidopsis by a miR156-targeted SPL transcription factor. Plant
1016 Cell *23*, 1512–1522.

1017 Guo, C., Xu, Y., Shi, M., Lai, Y., Wu, X., Wang, H., Zhu, Z., Poethig, R.S., and Wu, G. (2017).
1018 Repression of miR156 by miR159 regulates the timing of the juvenile-to-adult transition in
1019 *Arabidopsis*. Plant Cell *29*, 1293–1304.

1020 Guo, X., Hou, X., Fang, J., Wei, P., Xu, B., Chen, M., Feng, Y., and Chu, C. (2013). The rice
1021 *GERMINATION DEFECTIVE 1*, encoding a B3 domain transcriptional repressor, regulates seed
1022 germination and seedling development by integrating GA and carbohydrate metabolism. The
1023 Plant Journal *75*, 403–416.

1024 He, J., Xu, M., Willmann, M.R., McCormick, K., Hu, T., Yang, L., Starker, C.G., Voytas, D.F.,
1025 Meyers, B.C., and Poethig, R.S. (2018). Threshold-dependent repression of *SPL* gene expression
1026 by miR156/miR157 controls vegetative phase change in *Arabidopsis thaliana*. PLoS Genet. *14*,
1027 e1007337.

1028 Huijser, P., and Schmid, M. (2011). The control of developmental phase transitions in plants.
1029 Development *138*, 4117–4129.

1030 Jang, I.-C., Chung, P.J., Hemmes, H., Jung, C., and Chua, N.-H. (2011). Rapid and Reversible Light-
1031 Mediated Chromatin Modifications of Arabidopsis *Phytochrome A* Locus. Plant Cell *23*, 459–
1032 470.

1033 Jing, Y., Guo, Q., and Lin, R. (2019). The B3-Domain Transcription Factor VAL1 Regulates the
1034 Floral Transition by Repressing *FLOWERING LOCUS T*. Plant Physiol. *181*, 236–248.

1035 Kagaya, Y., Ohmiya, K., and Hattori, T. (1999). RAV1, a novel DNA-binding protein, binds to
1036 bipartite recognition sequence through two distinct DNA-binding domains uniquely found in
1037 higher plants. Nucleic Acids Research *27*, 470–478.

1038 Kim, K.-C., Lai, Z., Fan, B., and Chen, Z. (2008). *Arabidopsis* WRKY38 and WRKY62 Transcription
1039 Factors Interact with Histone Deacetylase 19 in Basal Defense. Plant Cell *20*, 2357–2371.

1040 Lawrence, E.H., Springer, C.J., Helliker, B.R., and Poethig, R.S. (2020). MicroRNA156-mediated
1041 changes in leaf composition lead to altered photosynthetic traits during vegetative phase
1042 change. New Phytologist.

1043 Leichty, A.R., and Poethig, R.S. (2019). Development and evolution of age-dependent defenses
1044 in ant-acacias. Proc Natl Acad Sci USA *116*, 15596–15601.

1045 Li, J., Wang, Z., Hu, Y., Cao, Y., and Ma, L. (2017). Polycomb Group Proteins RING1A and RING1B
1046 Regulate the Vegetative Phase Transition in Arabidopsis. Frontiers in Plant Science *8*, 867.

1047 Lopez-Vernaza, M., Yang, S., Müller, R., Thorpe, F., de Leau, E., and Goodrich, J. (2012).
1048 Antagonistic Roles of SEPALLATA3, FT and FLC Genes as Targets of the Polycomb Group Gene
1049 CURLY LEAF. PLOS ONE *7*, e30715.

1050 Mao, Y.-B., Liu, Y.-Q., Chen, D.-Y., Chen, F.-Y., Fang, X., Hong, G.-J., Wang, L.-J., Wang, J.-W., and
1051 Chen, X.-Y. (2017). Jasmonate response decay and defense metabolite accumulation
1052 contributes to age-regulated dynamics of plant insect resistance. Nature Communications *8*,
1053 13925.

1054 Molitor, A.M., Bu, Z., Yu, Y., and Shen, W.-H. (2014). Arabidopsis AL PHD-PRC1 Complexes
1055 Promote Seed Germination through H3K4me3-to-H3K27me3 Chromatin State Switch in
1056 Repression of Seed Developmental Genes. PLOS Genetics *10*, e1004091.

1057 Ossowski, S., Schneeberger, K., Clark, R.M., Lanz, C., Warthmann, N., and Weigel, D. (2008).
1058 Sequencing of natural strains of Arabidopsis thaliana with short reads. Genome Res *18*, 2024–
1059 2033.

1060 Pico, S., Ortiz-Marchena, M.I., Merini, W., and Calonje, M. (2015). Deciphering the role of
1061 Polycomb Repressive Complex 1 (PRC1) variants in regulating the acquisition of flowering
1062 competence in Arabidopsis. Plant Physiology *168*, 1286–1297.

1063 Qüesta, J.I., Song, J., Geraldo, N., An, H., and Dean, C. (2016). *Arabidopsis* transcriptional
1064 repressor VAL1 triggers Polycomb silencing at *FLC* during vernalization. Science *353*, 485–488.

1065 Ronemus, M., Vaughn, M.W., and Martienssen, R.A. (2006). MicroRNA-Targeted and Small
1066 Interfering RNA–Mediated mRNA Degradation Is Regulated by Argonaute, Dicer, and RNA-
1067 Dependent RNA Polymerase in *Arabidopsis*. Plant Cell *18*, 1559–1574.

1068 RStudio Team (2020). RStudio: Integrated Development Environment for R (Boston, MA:
1069 RStudio, PBC).

1070 Sasnauskas, G., Kauneckaitė, K., and Siksnys, V. (2018). Structural basis of DNA target
1071 recognition by the B3 domain of Arabidopsis epigenome reader VAL1. Nucleic Acids Research
1072 *46*, 4316–4324.

1073 Schindelin, J., Arganda-Carreras, I., Frise, E., Kaynig, V., Longair, M., Pietzsch, T., Preibisch, S.,
1074 Rueden, C., Saalfeld, S., Schmid, B., et al. (2012). Fiji: an open-source platform for biological-
1075 image analysis. Nature Methods *9*, 676–682.

1076 Schneeberger, K., Ossowski, S., Lanz, C., Juul, T., Petersen, A.H., Nielsen, K.L., Jorgensen, J.E.,
1077 Weigel, D., and Andersen, S.U. (2009). SHOREmap: simultaneous mapping and mutation
1078 identification by deep sequencing. Nat Methods *6*, 550–551.

1079 Serivichyaswat, P., Ryu, H.S., Kim, W., Kim, S., Chung, K.S., Kim, J.J., and Ahn, J.H. (2015).
1080 Expression of the floral repressor miRNA156 is positively regulated by the AGAMOUS-like
1081 proteins AGL15 and AGL18. Mol Cells *38*, 259–266.

1082 Shannon, P., Markiel, A., Ozier, O., Baliga, N.S., Wang, J.T., Ramage, D., Amin, N., Schwikowski,
1083 B., and Ideker, T. (2003). Cytoscape: A Software Environment for Integrated Models of
1084 Biomolecular Interaction Networks. Genome Research *13*, 2498–2504.

1085 Suzuki, M., Kao, C.Y., and McCarty, D.R. (1997). The conserved B3 domain of VIVIPAROUS1 has a
1086 cooperative DNA binding activity. Plant Cell *9*, 799–807.

1087 Suzuki, M., Wang, H.H.-Y., and McCarty, D.R. (2007). Repression of the *LEAFY COTYLEDON 1/B3*
1088 Regulatory Network in Plant Embryo Development by *VP1/ABSCISIC ACID INSENSITIVE 3-LIKE* B3
1089 Genes. Plant Physiol. *143*, 902–911.

1090 Telfer, A., Bollman, K.M., and Poethig, R.S. (1997). Phase change and the regulation of trichome
1091 distribution in *Arabidopsis thaliana*. Development *124*, 645–654.

1092 Tian, R., Wang, F., Zheng, Q., Niza, V.M.A.G.E., Downie, A.B., and Perry, S.E. (2020). Direct and
1093 indirect targets of the arabidopsis seed transcription factor ABSCISIC ACID INSENSITIVE3. The
1094 Plant Journal *103*, 1679–1694.

1095 Tsukagoshi, H., Morikami, A., and Nakamura, K. (2007). Two B3 domain transcriptional
1096 repressors prevent sugar-inducible expression of seed maturation genes in *Arabidopsis*
1097 seedlings. Proc Natl Acad Sci USA *104*, 2543–2547.

1098 Veerappan, V., Wang, J., Kang, M., Lee, J., Tang, Y., Jha, A.K., Shi, H., Palanivelu, R., and Allen,
1099 R.D. (2012). A novel HSI2 mutation in Arabidopsis affects the PHD-like domain and leads to
1100 derepression of seed-specific gene expression. Planta *236*, 1–17.

1101 Wang, F., and Perry, S.E. (2013). Identification of direct targets of FUSCA3, a key regulator of
1102 Arabidopsis seed development. Plant Physiology *161*, 1251–1264.

1103 Wang, L., Zhou, C.-M., Mai, Y.-X., Li, L.-Z., Gao, J., Shang, G.-D., Lian, H., Han, L., Zhang, T.-Q.,
1104 Tang, H.-B., et al. (2019). A spatiotemporally regulated transcriptional complex underlies
1105 heteroblastic development of leaf hairs in Arabidopsis thaliana. The EMBO Journal *38*, e100063.

1106 Weber, E., Engler, C., Gruetzner, R., Werner, S., and Marillonnet, S. (2011). A Modular Cloning
1107 System for Standardized Assembly of Multigene Constructs. PLOS ONE *6*, e16765.

1108 Wei, Q., Ma, C., Xu, Y., Wang, T., Chen, Y., Lü, J., Zhang, L., Jiang, C.-Z., Hong, B., and Gao, J.
1109 (2017). Control of chrysanthemum flowering through integration with an aging pathway.
1110 Nature Communications *8*, 829.

1111 Werner, S., Engler, C., Weber, E., Gruetzner, R., and Marillonnet, S. (2012). Fast track assembly
1112 of multigene constructs using Golden Gate cloning and the MoClo system. Bioeng Bugs *3*, 38–
1113 43.

1114 Wu, G., and Poethig, R.S. (2006). Temporal regulation of shoot development in *Arabidopsis*
1115 *thaliana* by miR156 and its target *SPL3*. Development *133*, 3539–3547.

1116 Wu, G., Park, M.Y., Conway, S.R., Wang, J.W., Weigel, D., and Poethig, R.S. (2009). The
1117 sequential action of miR156 and miR172 regulates developmental timing in *Arabidopsis*. Cell
1118 *138*, 750–759.

1119 Wu, G., Rossidivito, G., Hu, T., Berlyand, Y., and Poethig, R.S. (2015). Traffic lines: new tools for
1120 genetic analysis in *Arabidopsis thaliana*. Genetics *200*, 35–45.

1121 Xie, Y., Zhang, Y., Han, J., Luo, J., Li, G., Huang, J., Wu, H., Tian, Q., Zhu, Q., Chen, Y., et al.
1122 (2018). The Intronic *cis* Element *SE1* Recruits *trans*-Acting Repressor Complexes to Repress the
1123 Expression of *ELONGATED UPPERMOST INTERNODE1* in Rice. Molecular Plant *11*, 720–735.

1124 Xu, M., Hu, T., Zhao, J., Park, M.Y., Earley, K.W., Wu, G., Yang, L., and Poethig, R.S. (2016a).
1125 Developmental functions of miR156-regulated *SQUAMOSA PROMOTER BINDING PROTEIN-LIKE*
1126 (*SPL*) genes in *Arabidopsis thaliana*. PLoS Genet. *12*, e1006263.

1127 Xu, M., Leichty, A.R., Hu, T., and Poethig, R.S. (2018). H2A.Z promotes the transcription of
1128 *MIR156A* and *MIR156C* in *Arabidopsis* by facilitating the deposition of H3K4me3. Development
1129 *145*, dev152868.

1130 Xu, M.L., Hu, T.Q., Smith, M.R., and Poethig, R.S. (2016b). Epigenetic regulation of vegetative
1131 phase change in *Arabidopsis*. Plant Cell *28*, 28–41.

1132 Xu, Y.M., Guo, C.K., Zhou, B.Y., Li, C.L., Wang, H.S., Zheng, B., Ding, H., Zhu, Z.J., Peragine, A.,
1133 Cui, Y.H., et al. (2016c). Regulation of vegetative phase change by SWI2/SNF2 chromatin
1134 remodeling ATPase BRAHMA. Plant Physiol *172*, 2416–2428.

1135 Yang, C., Bratzel, F., Hohmann, N., Koch, M., Turck, F., and Calonje, M. (2013a). VAL- and
1136 AtBMI1-Mediated H2Aub Initiate the Switch from Embryonic to Postgerminative Growth in
1137 Arabidopsis. Current Biology *23*, 1324–1329.

1138 Yang, H., Howard, M., and Dean, C. (2014). Antagonistic Roles for H3K36me3 and H3K27me3 in
1139 the Cold-Induced Epigenetic Switch at Arabidopsis FLC. Current Biology *24*, 1793–1797.

1140 Yang, L., Xu, M., Koo, Y., He, J., and Poethig, R.S. (2013b). Sugar promotes vegetative phase
1141 change in *Arabidopsis thaliana* by repressing the expression of *MIR156A* and *MIR156C*. Elife *2*,
1142 e00260.

1143 Yu, S., Cao, L., Zhou, C.M., Zhang, T.Q., Lian, H., Sun, Y., Wu, J.Q., Huang, J.R., Wang, G.D., and
1144 Wang, J.W. (2013). Sugar is an endogenous cue for juvenile-to-adult phase transition in plants.
1145 Elife *2*, e00269.

1146 Yuan, L., Song, X., Zhang, L., Yu, Y., Liang, Z., Lei, Y., Ruan, J., Tan, B., Liu, J., and Li, C. (2020). The
1147 transcriptional repressors VAL1 and VAL2 recruit PRC2 for genome-wide Polycomb silencing in
1148 Arabidopsis. Nucleic Acids Research.

1149 Yuan, W., Luo, X., Li, Z., Yang, W., Wang, Y., Liu, R., Du, J., and He, Y. (2016). A cis cold memory
1150 element and a trans epigenome reader mediate Polycomb silencing of FLC by vernalization in
1151 Arabidopsis. Nature Genetics *48*, 1527–1534.

1152 Zeng, X., Gao, Z., Jiang, C., Yang, Y., Liu, R., and He, Y. (2020). HISTONE DEACETYLASE 9
1153 Functions with Polycomb Silencing to Repress *FLOWERING LOCUS C* Expression. Plant Physiol.
1154 *182*, 555–565.

1155 Zhao, H., Lin, K., Ma, L., Chen, Q., Gan, S., and Li, G. (2020). Arabidopsis NUCLEAR FACTOR Y A8
1156 inhibits the juvenile-to-adult transition by activating transcription of MIR156s. Journal of
1157 Experimental Botany *71*, 4890–4902.

1158 Zhou, Y., Tan, B., Luo, M., Li, Y., Liu, C., Chen, C., Yu, C.-W., Yang, S., Dong, S., Ruan, J., et al.
1159 (2013). HISTONE DEACETYLASE19 interacts with HSL1 and participates in the repression of seed
1160 maturation genes in Arabidopsis seedlings. Plant Cell *25*, 134–148.

1161 Zhou, Y., Romero-Campero, F.J., Gómez-Zambrano, Á., Turck, F., and Calonje, M. (2017). H2A
1162 monoubiquitination in Arabidopsis thaliana is generally independent of LHP1 and PRC2 activity.
1163 Genome Biology *18*, 69.

1164

1165